ASRL TR 1013

THE EFFECT OF FREE STREAM TURBULENCE AND VORTICITY ON THE RADIATIVE SOUND FIELD OF A FREE JET

78.P #/60

ROBERT D. SMITH

August 1963

MASSACHUSETTS INSTITUTE OF TECHNOLOGY
Department of Aeronautics and Astronautics
Aeroelastic and Structures Research Laboratory

National Aeronautics and Space Administration
Grant NsG-31-60

ABSTRACT

This work has as its objective the experimental examination of the changes which occur in the rms amplitude and the power spectral density of the radiative sound field of a round free jet of 0.5 inch diameter with the following velocity fields imposed at the jet nozzle exit.

(a) A vortex pair

(b) Free stream turbulence

(c) A vortex pair and free stream turbulence

(d) Turbulent wakes containing a Karman vortex street with 3.0 Kc. and 5.7 Kc. as frequencies of vortex emission.

Most of the tests were made for a jet nozzle exit Mach number of 0.8 with the rms amplitude and far field power spectra measured in the frequency range from 0.5 Kc. to 15.0 Kc.

The greatest factors of increase in power spectra occur in cases a and d and are 1.39 and 1.62 respectively. In case c the power spectra has a factor of maximum decrease of 0.853. This effect is of interest in jet engine noise reduction applications and is recommended for further study. In all four cases, various types of asymmetry, relative to the axis of the jet, were found in the power spectra. The asymmetries associated with cases a and b were found to be opposite.

In case d it was found that the frequency associated with the peak value of the power spectra had increased by 1.03 Kc. above

that associated with no imposed velocity field at the nozzle exit plane. It is felt that further experiments in this area may lead to an idea of the finer details of the sound production process.

ACKNOWLEDGEMENTS

The experiments described here were carried out within the Aeroelastic and Structures Research Laboratory of the Department of Aeronautics and Astronautics at the Massachusetts Institute of Technology. The work was supported by a grant from the National Aeronautics and Space Administration.

The author wishes to express his appreciation and gratitude to Professor Mollo-Christensen for much patience and constructive supervision.

Acknowledgements are also due to Mr. Fred Merlis for his assistance with and care of the complex electronic equipment involved in the experiments.

TABLE OF CONTENTS

LIST OF FIGURES

LIST OF SYMBOLS

a	Radius of the rigid body core of a circular vortex
b	Semi-distance between the centers of the vortices composing the vortex pair
c	Radius of the jet nozzle for a given point z along the jet axis
d	Diameter of the jet nozzle at the nozzle exit plane
D	Diameter of cylinder used to produce the Karman vortex street
f	Temporal frequency in cycles/sec.
$\hat{i}$, $\hat{j}$	Unit vectors along the x and y axes respectively
N	Vortex emission frequency associated with the Karman vortex street
p	Thermodynamic pressure
r	Magnitude of the position vector from the origin of coordinates to a point in space
$\hat{r}$, $\hat{\theta}$	Unit vectors associated with cylindrical coordinates in the nozzle exit plane
S	Dimensionless Frequency
v_x, v_y	Cartesian vector components of the velocity fluctuation field
V_r , V_θ , V_z	Components of the mean velocity field in cylindrical coordinates
$V_{\theta m}$	Magnitude of the induced velocity at the edge of the rigid body core of a circular vortex
x, y	Cartesian coordinates along axes perpendicular to the axis of the jet
z	Cartesian coordinate along the axis of the jet
α	Angle of attack of the airfoils of the airfoil type vortex generator

β	Angle subtended by the position vector and the z axis
ρ	Thermodynamic density
ϕ_o	Power spectral density of the radiative pressure fluctuation with no devices in the stilling section of the jet nozzle
ϕ_{xz}, ϕ_{yz}	Power spectral density of the radiative pressure fluctuation due to a device in the stilling section or jet nozzle and measured in the xz and yz planes respectively
ω	Magnitude of the vorticity vector associated with a circular vortex
Ω	Angular velocity of the rigid body core of a circular vortex

CHAPTER 1

INTRODUCTION

In recent years much effort has been concentrated in the study of jet noise both from the viewpoint of gaining an understanding of the production of sound radiation from a turbulent gas flow and also for the immediate purpose of reducing the undesirable noise generated by the engines of modern jet aircraft.

To this latter end, several types of jet noise suppressors have been designed which reduce the peak noise by at most 10 db. with some losses, however, in overall engine performance.

With regard to a basic understanding of the sound production process, there exists a theory established by M. J. Lighthill (Ref. 5, 6) and elaborated upon by others which is in fair agreement with the many experiments that have been performed. Some of these experiments (Ref. 4, 10) resulted in measurements, for given velocity and temperature fields at the exit of a round jet nozzle, of the mean velocity field and rms amplitude, power spectral density, and space-time correlation coefficient associated with the intensity of turbulence in the free shear layer. Measurements were also made of the power spectral density and directivity pattern of the pressure fluctuations associated with the radiative sound field.

It would be of interest, in the light of the above measurements, to observe in some detail the alterations induced in the radiative sound field, or far field, due to small changes in say the velocity field at the exit of the jet nozzle. Such alterations in the far field can be best observed via measurements of a statistical quantity such as the power spectral density of the radiative pressure fluctuation.

The consideration of the relative magnitudes of such changes may lead to a greater insight into the finer details of the process in which the diffusive kinetic energy of the turbulent fluctuations is converted into the radiative energy of sound.

On a more utilitarian level, such considerations may suggest the means by which a more effective reduction in jet engine noise may be accomplished.

Our objective then is to generate small changes of known magnitude in the velocity field at the exit of the jet nozzle and to note the alterations which occur in the rms amplitude and power spectral density of the radiative pressure fluctuation at various points in the far field.

CHAPTER 2

GENERAL CONSIDERATIONS

2.1 The Flow Field of a Round Subsonic Free Jet

Before embarking on a study of the dynamics of the sound generation process, it would be well to consider the viscous flow field generated by a free subsonic jet of air emerging from a round converging nozzle into a still atmosphere. This flow field is best described, for the purposes of the present discussion, by cylindrical coordinates (see Fig. 1). It will be assumed that the mean flow at the nozzle exit plane ($z=0$) is described by $V_z = V(r)$, $V_r = 0$, $V_\theta = 0$ and that the temperature profile there is rectangular.

As the high speed air near $r = \frac{d}{2}$ comes in contact with the still air of the atmosphere, a region of large velocity gradient called the free shear layer is produced. This free shear layer can be thought of, via the Taylor-Helmholtz instability, as a cylindrical vortex sheet. This flow is still, however, considered laminar. In the region $0 < z < d$, which shall be denoted as Region I, molecular viscosity causes diffusion of the vortices in the cylindrical vortex sheet causing the width of the shear layer to increase to a point where the motion is unstable to the small disturbances which always exist in a fluid

flow. In a region of this point, then, a transition to turbulent flow is achieved in the free shear layer. If the boundary layer at z = 0 is already turbulent, a transition still occurs in Region I. This transition, however, is to a turbulence having a power spectral density with a different functional form.

In the region $d < z \lesssim 5d$, which we define as Region II, the width of the laminar core of the jet decreases to zero as shown in Fig. 2. In this region, the measurable statistical moments of the turbulent field exhibit a similarity relative to conical coordinates.

Beyond z = 5d a transition occurs to fully developed turbulent jet flow, which is characterized by the familiar bell-shaped velocity profile. Most of the energy in the radiative sound field has its source in Regions I and II.

2.2 The Sound Field Produced by a Round Subsonic Free Jet

In the theory formulated by M. J. Lighthill, the radiative sound produced by the free shear layer of a round free subsonic jet of air discharging into a still atmosphere would be equivalently produced by an axisymmetric distribution of radiating quadrupoles occupying the volume of space associated with the free shear layer and being convected at a speed approximately one half of the exit velocity of the jet.

In this theory, the radiated sound is seen to be generated by the fluctuating Reynolds stresses $\rho v_i v_j$ in the free shear layer. Since $\rho v_i v_j$ can also be thought of as a momentum flux tensor, the generation of radiated sound can be associated with varying rates of momentum flux across surfaces in the turbulent velocity field. For low subsonic Mach numbers $\rho v_i v_j$ is approximately the amplitude of the equivalent quadrupole strength per unit volume denoted by T_{ij}.

As given in Lighthill's theory, the radiative pressure fluctuation $\Delta p(\bar{r}, t)$, at a point $\bar{r}$ in the atmosphere, due to a single convected eddy in the free shear layer is given by:

$$\Delta p(\bar{r}, t) = \sum_{i=1}^{3}\sum_{j=1}^{3} \frac{x_i x_j V_\ell \ddot{T}_{ij}(t')}{4\pi a_0^2 |\bar{r}|^3 (1 - M_0 \cos\theta)^3}$$

$$t' = t - \frac{|\bar{r}|}{a_0} \qquad \dot{T}_{ij} = \frac{\partial}{\partial t'}(T_{ij}) \qquad r = \left\{ \sum_{i=1}^{3} x_i x_j \right\}^{\frac{1}{2}} \qquad M_0 = \frac{U_0}{a_0} \qquad (2.1)$$

a_0 = the speed of sound in still atmosphere

U_0 = the velocity of convection of the eddy relative to the still atmosphere

θ = the angle subtended by $\bar{r}$ and the z axis

V_ℓ = the volume occupied by the eddy

An eddy in the free shear layer will be defined as a region of the fluid, convected at a speed U_0 by the mean flow, in which the spatial autocorrelation coefficient, taken in a reference frame moving with the eddy, is relatively close to one. This picture can be idealized somewhat by saying that T_{ij} inside the eddy is well correlated but is completely uncorrelated with T_{ij} outside the eddy. This eddy can then be replaced by a single quadrupole radiator as indicated by Equation 2.1.

The purpose of exhibiting Equation 2.1 is to illustrate the fact that the radiative pressure fluctuation $\Delta p(\bar{r}, t)$ has its source in the second retarded time variation of the fluctuating Reynolds stresses.

Now the coefficients in the equations of motion which govern the temporal variations of $\rho v_i v_j$ and hence through Equation 2.1 the radiative pressure fluctuation $\Delta p(\bar{r}, t)$, are functions of the mean velocity distrubition V_z, V_r, V_θ . Thus the production of alterations in $\Delta p(\bar{r}, t)$ should be possible via suitable changes in V_z, V_r, V_θ which can be produced by given changes in V_z, V_r, V_θ evaluated at z = 0, the nozzle exit plane. If such changes in $V_z|_{z=0}, V_r|_{z=0}, V_\theta|_{z=0}$ are very small in comparison with $V_z|_{z=0}$, then observation of the consequent alterations in the rms amplitude and the power spectral density of $\Delta p(\bar{r}, t)$ can lead to an idea of the sensitivity of the sound radiation producing mechanism to small changes in the velocity field at the nozzle exit plane.

Since $V_z|_{z=0}$ is very large, small changes in it will lead to trivial results. Measureable results may be obtained, however, by giving $V_r|_{z=0}$ and $V_\theta|_{z=0}$ small but finite values with $V_z|_{z=0}$ held fixed. This may be accomplished by the creation of a distribution of vorticity such as that due to a vortex pair at the nozzle exit plane.

Another possible way of altering $\Delta p(\bar{r}, t)$ due to changes in $\ddot{T}_{ij}$ is via the interaction with the free shear layer of a field of turbulence convected downstream, across the nozzle exit

plane, into the laminar core of the jet. A specialization of this would involve the use of a semi-turbulent field such as the turbulent wake produced when a flow moves past a cylinder for large enough Reynolds number. Such a wake is composed of a field of turbulent fluctuations superimposed on a set of large scale regular motions termed as the Karman vortex street. To this, a temporal frequency of vortex emission, denoted by N, may be assigned. This frequency may be varied by suitable adjustments of the flow variables U , ν and the cylinder diameter D as is shown below.

$$\frac{ND}{\nu} = f\left(\frac{UD}{\nu}\right) \tag{2.2}$$

U = the free stream velocity of the flow past the cylinder

ν = the kinematic viscosity of the fluid.

A plot of f versus the Reynolds number based on cylinder diameter may be found in Reference 11.

Two possible values for N which would be of spectral interest are 3.0 Kc. and 5.7 Kc. The former frequency is approximately that associated with the peak value of the power spectral density of $\Delta p(\bar{r}, t)$, while the latter is associated with the maximum of the power spectral density of the turbulent intensity in the free shear layer at z = 4d, half way to the downstream end of the laminar core of the jet, for a jet nozzle exit diameter of 0.5 inches.

The objective, then, will be a comparison of the rms amplitude and power spectral density of the radiative pressure fluctuation $\Delta p(\bar{r},t)$, contained in the frequency range of .5 Kc. to 15.0 Kc., for the following velocity field configurations imposed in the nozzle exit plane:

(a) A vortex pair

(b) Free stream turbulence

(c) The superposition of a vortex pair and free stream turbulence

(d) Turbulent wakes containing a Karman vortex street with 3.0 Kc. and 5.6 Kc. as frequencies of vortex emission.

Since the frequency range .5 Kc. to 15.0 Kc., denoted as the low frequency emission range, contains almost all of the energy associated with the radiative pressure fluctuation, any changes in $\Delta p(\bar{r},t)$ produced by the above condigurations would be easily detected. Since it contains almost all of the energy in $\Delta p(\bar{r},t)$, the above frequency range contains almost all of the undesirable jet noise and hence is of interest in jet engine noise reduction applications.

2.3 Analysis of the Various Velocity Fields Produced at the Nozzle Exit

In this section an approximate analysis will be made of the velocity field induced at the nozzle exit plane due to the convection across this plane of a vortex pair. The object of the analysis will be the estimation of the upper bounds of $V_r|_{z=0}$ and $V_\theta|_{z=0}$ induced by the vortex pair. Also the effect of

the jet nozzle on fields of turbulence convected through it will be briefly discussed.

If the vortex generator which generates the vortex pair is mounted slightly upstream of the nozzle entrance plane, for reasons to be given in Section 3.2, then one must be able to relate paramaters associated with the velocity field in the nozzle entrance plane with corresponding parameters associated with the velocity field at the nozzle exit plane.

To this end, the vortex pair in the nozzle exit plane is represented by two circular vortices situated at $r = b$, $\theta = \frac{\pi r}{a}$ and $r = b$, $\theta = -\frac{\pi r}{a}$ as shown, along with the associated streamline pattern, in Fig. 3. It is also seen from Fig. 3 that the vorticity vectors associated with the vortex pair are equal in magnitude but opposite in sign thereby giving a net circulation of zero over the whole nozzle exit plane.

A single circular vortex at the origin of polar coordinates in an infinite incompressible medium of density ρ has the following distrubitions of vorticity, velocity, and pressure

$$|\nabla \times \bar{V}| = \begin{cases} \omega & r < a \\ 0 & r > a \end{cases} \tag{2.3}$$

$$V_\theta = \begin{cases} \frac{\omega r}{2} & r \leq a \\ \frac{\omega a^2}{2r} & r \geq a \end{cases} \tag{2.4}$$

$$V_r = 0$$

$$P = \begin{cases} p_\infty - \frac{\rho \omega^2}{8}(r^2 - 2a^2) & r \leq a \\ p_\infty - \frac{\rho \omega^2}{8}\left(\frac{a^4}{r^2}\right) & r \geq a \end{cases} \tag{2.5}$$

where a is the radius of the rigid body core, outside of which there is only potential motion. The lower bound of a is $\frac{2}{\omega}\left(\frac{p_\infty}{\rho}\right)^{\frac{1}{2}}$

due to the fact that $\{p(r) \mid r=0\} \geq 0$. It is also to be noted that while the pressure and velocity fields are continuous at r = a, the vorticity field is not.

Suppose that such a circular vortex is generated at the nozzle entrance plane with its center coinsiding with the z axis as it is convected downstream to the nozzle exit plane. In order to relate the angular velocity $\frac{\omega_0}{2}$ and the radius a_0 of the rigid body core at the nozzle entrance plane in a simple manner to the corresponding values $\frac{\omega_1}{2}$ and a_1 in the nozzle exit plane, the circulations in the two planes would have to be equated.

$$\Gamma_0 \equiv \pi a_0^2 \omega_0 = \Gamma_1 \equiv \pi a_1^2 \omega_1$$

This results in:

$$a_0^2\left(\frac{\omega_0}{2}\right) = a_1^2\left(\frac{\omega_1}{2}\right) \qquad (2.6)$$

To make such a step one must assume that no frictional forces act on the circular vortex as it is convected through the nozzle and that a is much less than c, the radius of the nozzle, for all z between the nozzle entrance and exit planes.

As the flow area in the convergent jet nozzle decreases a also decreases and the rigid body core undergoes stretching so as to preserve continuity of mass. Since angular momentum must also be conserved (no frictional forces acting) the angular velocity $\frac{\omega}{a}$ of the rigid body core must increase as shown in Equation 2.6. It will also be assumed, as an approximation, that a decreases at the same rate as does c. That is:

$$\frac{a_0}{a_1} = \frac{c_0}{c_1} \tag{2.7}$$

Denoting the angular velocity of the rigid body core as Ω, one gets:

$$\Omega_1 = \Omega_0 \left(\frac{c_0}{c_1}\right)^2 \tag{2.8}$$

The maximum value of V_θ, which occurs at r = a, in the nozzle exit plane becomes:

$$V_{\theta M} = \frac{\Omega_0 a_0 c_0}{c_1} \tag{2.9}$$

While the minimum pressure in the nozzle exit plane occurs at r = 0 and is given by:

$$p = p_\infty - \frac{\rho \omega_1^2 a_1^2}{4} \tag{2.10}$$

In the nozzle exit plane the pressure is atmospheric and is denoted by p_A. If p_∞ is set equal to p_A, one gets:

$$\left(\frac{p_{min}}{p_A}\right) = 1 - \frac{\rho}{p_A}(\Omega_0 a_0)^2 \left(\frac{c_0}{c_1}\right)^2 \tag{2.11}$$

Inherent in this statement, is the assumption that while ρ in the nozzle exit plane is not equal to atmospheric density, it is constant across the nozzle exit plane.

If the possibilities of the aforementioned flow were to be considered in terms of jet engine noise reduction applications, involving the replacement of the convergent nozzle by a jet engine nozzle, then the paramenter γ defiened by

$$\tan \gamma = \frac{V_{\theta M}}{V_z|_{z=0}} \tag{2.12}$$

would be of great importance due to the fact that a large value of γ would involve an appreciable reduction in the thrust produced by the engine.

We will now make the approximation that the parameters Ω_1, $V_{\theta M}$, $\left(\frac{P_{MIN}}{P_A}\right)$, and γ, evaluated in the nozzle exit plane, for <u>each</u> vortex of the vortex pair, with ω_0 and a_0 associated with each vortex at the nozzle entrance plane, are given by Equations 2.8, 2.9, 2.11 and 2.12 which were arrived at via considerations pertaining to a single circular vortex convected along the z axis. A factor, on which the accuracy of the above approximation depends, is the degree to which $a_1 \ll c_1$ and $a_1 \ll b_1$ (see Fig. 3). Also inherent in the above approximation is the assumption that the configurations, as shown in Fig. 3, in the nozzle exit plane is the same, except for a change of scale, as that in the nozzle entrance plane. This means that

$$\frac{a_0}{a_1} = \frac{b_0}{b_1} = \frac{c_0}{c_1}$$

and that the centers of the rigid body cores remain in the yz plane. The latter assumption is, in general, incorrect. This is due to the fact that if the vortex pair, in the nozzle entrance plane, has the geometry shown in Fig. 3, then each vortex will initially induce a velocity of

$$\frac{\omega_o a_o^2 \hat{\lambda}}{4 b_o}$$

at the center of the other. Other components of velocity are also induced at the center of each vortex (Ref. 9) due to the presence of the cylindrical wall. This is best visualized by replacing the region $r \geq c$ by a velocity field due to a set of image vortices. The velocity induced by the presence of the cylindrical wall is given below for the case of a single circular vortex initially situated in the cylinder, in the nozzle entrance plane, at $r = b_o$ and $\Theta = \frac{\pi}{2}$ (see Fig. 3).

$$\bar{V} = \frac{a_o^2 \omega_o b_o \hat{\theta}}{2(c_o^2 - b_o^2)} \tag{2.13}$$

Or in cartesian coordinates:

$$\bar{V} = \frac{a_o^2 \omega_o b_o}{2(c_o^2 - b_o^2)} \left\{ \hat{y} \cos\Theta - \hat{\lambda} \sin\Theta \right\} \tag{2.14}$$

This means that under the influence of the cylindrical wall, a single vortex initially situated at $r = b_o$, for any value of Θ, will move in a circular path of radius b_o about the z axis. If all effects due to the interaction of the image vortices are neglected, the total initial induced velocity,

in the nozzle entrance plane, at the center of each vortex of the vortex pair becomes

$$\overline{V}_T = \frac{a_o^2 \omega_o b_o \cos\theta}{2(c_o^2 - b_o^2)}\hat{j} + \frac{\omega_o a_o^2}{2}\left\{\frac{1}{2b_o} - \frac{b_o \sin\theta}{(c_o^2 - b_o^2)}\right\}\hat{\lambda} \qquad (2.15)$$

The maximum and minimum values of $|\overline{V}_T|$ occur at $\theta = -\frac{\pi}{2}$ and $\theta = \frac{\pi}{2}$ respectively with the corresponding magnitudes given by:

$$|\overline{V}_T|_{MAX} = \frac{a_o^2 \omega_o}{4b_o}\left\{\frac{c_o^2 + b_o^2}{c_o^2 - b_o^2}\right\} \qquad (2.16)$$

$$|\overline{V}_T|_{MIN} = \frac{a_o^2 \omega_o}{4b_o}\left\{\frac{3b_o^2 - c_o^2}{c_o^2 - b_o^2}\right\} \qquad (2.17)$$

If $|\overline{V}_T|_{MAX}$ can be made much less than the average value that $V_z|_{z=0}$ assumes between the nozzle entrance and exit planes via suitable adjustments of a_o, ω_o, and b_o, then the configurations in the nozzle entrance and exit planes will have approximate geometrical similarity.

In addition to obtaining an upper bound for $V_r|_{z=0}$ and $V_\theta|_{z=0}$ in the form of $V_{\theta M}$, one must obtain some idea of the effect exerted on the longitudinal and lateral turbulent fluctuations in the turbulent wakes convected through the convergent jet nozzle.

If a turbulent wake producing device, such as a cylinder, is mounted somewhere in the convergent jet nozzle upstream of the nozzle exit plane, then it will be found that the sharp contraction in flow area and the consequent acceleration

experienced by the mean flow, in the nozzle, causes a substantial decrease in the relative intensity of the turbulent fluctuations in the wake (see Ref. 11, pp. 68-75).

The approximate ratios of the longitudinal and lateral turbulent intensities in the nozzle exit plane to those in the nozzle entrance plane are

$$A = \left.\frac{\left\{\overline{v_z^2}\right\}^{\frac{1}{2}}}{V_z}\right|_{z=0} \Big/ \left.\frac{\left\{\overline{v_z^2}\right\}^{\frac{1}{2}}}{V_z}\right|_{z=-z_0} = \left\{\frac{3}{4} h^{-2}\left(\ln 4h^3 - 1\right)\right\}^{\frac{1}{2}} \left(\frac{V_z|_{z=-z_0}}{V_z|_{z=0}}\right) \qquad (2.18)$$

and

$$B = \left.\frac{\left\{\overline{v_r^2 + v_\theta^2}\right\}^{\frac{1}{2}}}{V_z}\right|_{z=0} \Big/ \left.\frac{\left\{\overline{v_r^2 + v_\theta^2}\right\}^{\frac{1}{2}}}{V_z}\right|_{z=-z_0} = \left\{\frac{3}{4} h\right\}^{\frac{1}{2}} \left(\frac{V_z|_{z=-z_0}}{V_z|_{z=0}}\right) \qquad (2.19)$$

respectively, where

$$h(z) = \left(\frac{r(z)}{r(0)}\right)^2$$

is denoted as the contraction ratio and v_r , v_θ and v_z are the turbulent velocity fluctuations in the r, θ , and z directions. The nozzle entrance plane is denoted by $z = -z_0$

It can be seen from the above that the suppression of the turbulent fluctuations is much more pronounced in the longitudinal direction and that the effect may be increased, up to a point, by mounting the particular device, which generates the wake, further upstream where r(z) is larger.

CHAPTER 3

DESCRIPTION OF EXPERIMENTAL APPARATUS

3.1 Flow Producing Apparatus

The Wright Brothers Wind Tunnel compressor (see Fig. 4) served as an air supply for the jet and had a capability of supplying one pound of air per second at 30 psi. gauge pressure. The air was then fed into a set of dryers, which kept its dewpoint below -20° C., so that it could be considered dry even after undergoing insentropic expansion in the jet nozzle. A variable bypass, immersed in a sandbox to attenuate unwanted vibrations and sound due to the compressor and valves, served to regulate the air supply. To further attenuate unwanted vibrations and sound, the air was passed through a flexible rubber hose before going to the settling chamber.

All experiments were performed with the jet in the "cold" condition. This means that no heaters were used and that the temperature of the air in the settling chamber was 26.6° C. during a run.

The settling chamber consisted of a 10 foot section of heavy cast iron pipe having a radius of 6 inches. Very high turbulent mixing was introduced in the first two feet of the

settling chamber so as to equalize both velocity and temperature in the air flow. This high level of turbulence was then reduced in the next 6 feet of the settling chamber via 5 sections of steel wool, each 6 inches thick, held between screens. The flow then proceeded to a straightening device, one foot long, made of finned steel tubing. The flow was then passed through three screens of decreasing mesh size and into the 18 inch stilling section.

Placed upstream of the straightening device, to avoid disturbing the flow in the stilling section, was a well filled with oil in which was immersed a thermometer used to measure the temperature of the flow in the settling chamber. The accuracy with which the thermometer could be read was $.5^{o}$ C.

The pressure in the settling chamber was measured by means of a mercury manometer which had an accuracy of 0.125 cm. Hg. The pressure reading did not vary more than 0.25 cm. Hg. during a run.

After leaving the stilling section, the flow passed through a brass jet nozzle, having an exit diameter of 0.5 inches, mounted at the termination of the pipe construction. The flow then passed through the anechoic chamber and was discharged through the jet catcher as shown in Fig. 4.

In the absence of obstructing devices in the jet nozzle or the stilling section, the boundary layer, on the nozzle wall, in the region of the nozzle exit was laminar due to the low turbulence level of the input flow to the nozzle and the fact that the nozzle wall was highly polished.

3.2 Vortex Generators

Two types of vortex generators were used, each producing a different velocity field at the nozzle exit plane. Each was mounted in the stilling section slightly upstream of the nozzle entrance plane, or in more exact terms, 18.31 inches upstream of the nozzle exit plane. This was done so as to maximize Ω_1 (see Equation 2.8) so that a magnitude may be given to $V_{\theta M}$ (see Equation 2.9) which is sufficient to cause measureable alterations in the radiative sound field. Such a mounting position also causes the relative intensity of the turbulent fluctuations, at the nozzle exit plane, in the wake produced by the device to be minimized (see Equations 18 and 19).

Since one would like to differentiate between the effect on $\Delta p(\bar{r},t)$ due to the velocity field of the vortex pair at the nozzle exit plane and the effect due to a field of turbulence convected across the nozzle exit plane, it would be of advantage to construct a vortex generator which produced a minimum of turbulence.

The generator, denoted as the airfoil type generator, is shown in Fig. 5. It consisted of three balsa NACA 4412 type airfoils, each having a 2.5 inch chord, mounted side by side on a 0.125 inch diameter steel rod. The angles of attack of the airfoils were equal in magnitude but consecutively opposite in sign so as to maximize ω_0 . The spans of the center and side panels were 5.56 inches and 3.0 inches respectively. For the purpose of reducing turbulence, the angles of attack of the

airfoils were kept below the angle at which the boundary layer on the upper surface of the airfoil becomes separated.

This angle was measured by placing a hot wire probe 0.5 inches aft of and 0.25 inches above the center of the trailing edge of the center panel in a flow having a free stream speed of 14.65 feet per second. While the output of the hot wire set was monitored on an oscilloscope, the angle of attack was slowly increased from zero until large fluctuations suddenly appeared. The aforementioned angle was noted as 11.96^{o} . In the actual runs, the upper bound for the angle of attack was set at 11.33^{o} . This is satisfactory in the light of the fact that the mean velocity in the stilling section is only 1.1 feet per second (corresponding to an exit Mach no. of .8).

To further reduce free stream turbulence in the flow across the nozzle exit plane, the side panels were fitted tightly against blasa fairings which fitted flush against the circular wall of the settling chamber.

The separation between the panels was adjusted so as to maximize ω_o . This was accomplished using a stroboscope (Strobotac Type 1531-A) manufactured by the General Radio Co. and a 0.375 inch diameter vortometer mounted 0.5 inches aft of the trailing edge as shown in Fig. 6. The vortometer, also shown in Fig. 6, consisted of two 0.312 inch thick balsa panels 0.156" x 0.141" mounted on an aluminum hub 0.0625 inches in diameter. The distance between consecutive airfoil panels, which produced a maximum ω_o , was found to be 0.0937 inches.

The van type vortex generator, shown in Fig. 7, was designed so that the combined effects on $\Delta p(\bar{r},t)$ of a vortex pair and free stream turbulence at the nozzle exit plane might be observed. This is reflected in the use of the relatively large maximum and minimum angles of attack of 42.0^{o} and -38.5^{o} respectively. Such large angles of attack are required because the sharp contraction in flow area in the jet nozzle causes a large decrease in the relative intensity of the turbulent fluctuations in the wake produced by the device. These fluctuations, upon reaching the nozzle exit plane, will be primarily in the lateral direction (see Equations 2.18 and 2.19).

3.3 Turbulence Generators

The turbulence generators, designed so that only the effect on $\Delta p(\bar{r},t)$ of a field of turbulence convected across the nozzle exit plane might be observed, were also divided into two groups.

The first type, denoted as the wing type turbulence generator, consisted of a flat plate type airfoil composed of 0.0312 inch thick soft aluminum sheet with a 12 inch span and a 2.5 inch chord. It was mounted at an angle of attack of -19.25^{o} at the same point in the stilling section as were the vortex generators. In light of its purpose, the device was not to produce a wake containing any large scale vortices of a regular nature, having components of the vorticity vector parallel to the z axis.

To ascertain the possible existance of such vortices, the device was mounted at an angle of attack of -19.25° in a flow having a free stream speed of 14.65 feet per second, and the wake was explored using the 0.375 inch diameter vortometer oriented in the manner shown in Fig. 7. No large scale vortices such as described above were found to exist in the wake for the aforementioned free stream speed. It is then assumed that no such distributions of vorticity will exist for any free stream speed less than 14.65 feet per second.

The second group of vortex generators consisted of two smooth wood cylinders each 0.078 inches in diameter. Each was mounted in the yz plane (see Fig. 1) by gluing its ends to the wall of the convergent jet nozzle at c = 0.605 inches and c = 0.439 inches. At an exit Mach number of 0.8, this produced vortex emission frequencies of 3.0 Kc. and 5.7 Kc. respectively.

It is also to be noted that, since the members of this latter group of turbulence generators are mounted at sections of smaller cross sectional diameter in the convergent nozzle than are the wing type turbulence generator and the vane type vortex generator, the resultant decrease in the relative intensity of the lateral and longitudinal turbulent fluctuations, while in passage through the remainder of the nozzle, will be considerably less.

3.4 Acoustical Apparatus

The jet nozzle discharged the flow into an 8x8x8 foot anechoic changer whose walls, ceiling, and floor were covered by a layer of one-inch thick fiberglass mats. On top of this was fastened a wave shaped layer of similar mats as shown in Fig. 4. To permit easy access to the chamber, the upstream wall consisted of a curtain of heavy cloth. This was deemed permissible because this wall, due to its orientation relative to the flow, received relatively little sound radiation.

A Bruel and Kjaer condenser microphone with an 0.5 inch diameter face was used for all measurements of the rms amplitude and the power spectral density of the radiative pressure fluctuation. This microphone had a flat frequency response, for axially impinging sound radiation, in the range from 20 cps to 35 Kc., and it had an rms signal-to-noise ratio well below 5×10^{-3}.

The microphone was hung from a horizontal boom which could be rotated about the x axis (see Fig. 1). The boom was positioned using a protractor mounted on it, and the microphone was positioned relative to the boom by the use of a plumb line hanging from the boom. This system involved a maximum error in microphone positioning of 0.1 inches.

3.5 Signal Processing System

The electrical signal, due to the pressure fluctuation on the face of the microphone, serves, after amplification (see Fig. 8) as the input to the wave form analyser (Donner Model No. 2102). This frequency selective device measures the relative average amplitudes and the frequencies of the Fourier components of the electrical signal, and is characterized by a constant power band pass of 25 cps with a frequency range from 30 cps to 50 Kc. After leaving this device, the signal passes through a linear averaging circuit and registers as a deflection of the pen in the Leeds and Northrup Speedomax Type G pen recorder. The frequency dial of the wave form analyser was mechanically linked via a system of chains and sprockets to the drive of the pen recorder. The pen recorder was then able to plot the square root of the power spectral density of the input to the wave analyser versus frequency. A built-in system of calibration was utilized to check for electrical drift in the various components of the signal processing system during a run.

In addition to being monitored on an oscilloscope, the input to the wave form analyser was also passed through a filter with adjustable band pass so that the rms amplitude of the radiative pressure fluctuation could be noted for the frequency range from 0.5 Kc. to 15.0 Kc. prescribed earlier.

CHAPTER 4

ANALYSIS AND DISCUSSION OF MEASUREMENTS PERTAINING TO THE VELOCITY FIELDS PRODUCED AT THE JET NOZZLE EXIT

Due to difficulties in making vorticity measurements in the stilling section, the angular velocity of the rigid body core of each member of the vortex pair, produced by the airfoil type vortex generator, was measured with the generator mounted in the test section of a wind tunnel in which was produced a uniform flow having a free stream speed of 14.65 feet per second. With the angles of attack of the airfoils set at $\pm$ 11.33° the aforementioned angular velocity was measured as 125 radians per second. This was done using the stoboscope with the 0.375 inch diameter vortometer mounted 0.5 inches aft of the trailing edge of the airfoils as shown in Fig. 7. If it is assumed that Ω_o , the angular velocity of the rigid body core 0.5 inches aft of the generator is directly proportional to the free stream velocity of the flow in which the generator is mounted, then the value of Ω_o in the stilling section, where the free stream velocity is 1.1 feet per second, can be found as 9.4 radians per second. The corresponding value of Ω_o for the vane type vortex generator is 5.75 radians per second.

The radius of the rigid body core, associated with Ω_0, was taken as the radius of the vortometer for both vortex generators.

Substitution of the parameters Ω_0 and a_0 as well as the geometry of the jet nozzle and vortex generators into Equations 2.7, 2.9, 2.11, 2.12, and 2.17 yields the parameters tabulated below:

Parameter	Airfoil Type Vortex Generator	Wing Type Turbulence Generator
a_0	0.187 inches	0.187 inches
a_1	0.0078 inches	0.0078 inches
b_0	2.56 inches	3.75 inches
b_1	0.106 inches	0.156 inches
c_0	6.0 inches	6.0 inches
c_1	0.25 inches	0.25 inches
Ω_0	9.4 radians/second	5.75 radians/second
Ω_1	5.41×10^3 radians/sec.	3.31×10^3 radians/sec.
$V_{\theta M}$	3.52 feet/second	2.16 feet/second
γ	0.234°	0.15°
$\lvert\bar{V}_T\rvert_{MAX}$	0.047 inches/second	0.0306 inches/second
$\lvert\bar{V}_T\rvert_{MIN}$	0.0215 inches/second	0.00375 inches/second
$\left(\frac{P_{MIN}}{P_A}\right)$	$1 - .102 \times 10^{-4}$	$1 - .401 \times 10^{-5}$

Since $V_r|_{z=0} \leq V_{\theta M} \leq 4$ feet/second and $V_\theta|_{z=0} \leq V_{\theta M} \leq 4$ feet/second the condition that $V_r|_{z=0}$ and $V_\theta|_{z=0}$ be very small in comparison to $V_z|_{z=0}$ is readily satisfied. This as well as the computed values of the ratio of minimum to atmospheric pressure at the nozzle exit, $\left(\frac{P_{MIN}}{P_A}\right)$, indicate that the presence of

the vortex pair in the nozzle exit plane has a negligible effect on the exit Mach number.

Using the computed values for $|\overline{V_T}|_{MAX}$, the assumption made in Section 2.3 regarding the geometrical similarity of the vortex configurations at the nozzle entrance and exit planes can be readily examined. If 18.31 inches is taken as the separation between such planes and 120 inches per second as the average value of $V_z|_{r=0}$ as the flow passes through the nozzle, then a passage time of 0.15 seconds for the mean flow is obtained. If it is assumed that the center of the rigid body core of a circular vortex, upon reaching the nozzle entrance plane, immediately obtains a velocity, parallel to this plane, of magnitude $|\overline{V_T}|_{MAX} = 0.047$ inches per second, then the maximum displacement of the center of the rigid body core, on reaching the nozzle exit plane, is 0.00705 inches. A comparison of this displacement with b_1 and c_1 justifies the assumption of geometrical similarity made in Section 2.3. This result as well as the fact that $a_0 \ll b_0$ and $a_0 \ll c_0$ serves to justify the main approximation of Section 2.3 which replaced the parameters Ω_1, $V_{\theta M}$, $\left(\frac{p_{MIN}}{p_A}\right)$, and Γ associated with each member of the vortex pair by the corresponding values given in Equations 2.8, 2.9, 2.11, and 2.12 which were arrived at via consideration of a single circular vortex convected along the z axis.

To give an idea of the suppression in the convergent jet nozzle of the relative intensities of the longitudinal and lateral turbulent fluctuations associated with the turbulent wakes produced by the vane type vortex generator and the various turbulence generators, the ratios of relative intensity A and B, specified analytically by Equations 2.18 and 2.19 are given below.

Device	Contraction Ratio	A	B
Vane type vortex generator	576.0	1.95×10^{-8}	2.65×10^{-2}
Wing type vortex generator	576.0	1.95×10^{-8}	2.65×10^{-2}
Cylinder type turbulence generator N=3.0 Kc.	5.86	4.51×10^{-4}	2.68×10^{-3}
Cylinder type turbulence generator N=5.7 Kc.	3.06	6.97×10^{-4}	1.94×10^{-3}

CHAPTER 5

ANALYSIS AND DISCUSSION OF MEASUREMENTS PERTAINING TO THE RADIATIVE SOUND FIELD

5.1 Introductory Remarks

Measurements were made of the rms amplitude and power spectral density of the pressure fluctuation $\Delta p(\vec{r},t)$ contained in the frequency range from 0.5 Kc. to 15.0 Kc. for various points in the radiative sound field, or far field, for the four nozzle exit plane velocity field configurations specified on page eight.

Since the changes in the rms amplitude and power spectral density, caused by each of the four specified velocity fields in the nozzle exit plane, could possibly be in the form of an asymmetry relative to the z axis, measurements made in the yz plane, in which the various vorticity and turbulence producing devices were mounted, were repeated in the xz plane. This had to be accomplished by rotating the generating device through 90 degress, due to the fact that the microphone and boom assembly was constrained to move only in the yz plane.

5.2 The Power Spectral Densities

In Figs. 9 to 29 are plotted the far field power spectra, in arbitrary units, associated with the four aforementioned nozzle exit plane velocity fields, versus the dimensionless frequency S defined by

$$S = (d)\ (f)/V_z|_{z=0}$$

for the S range of 0.0242 to 0.727 which corresponds to a temporal frequency range of 0.5 Kc. to 15.0 Kc. All power spectra shown are associated with an exit nozzle diameter of 0.5 inches and an exit Mach number of 0.8. The power spectra measured for a given (r, θ) point in the xz and yz planes will be denoted by ϕ_{xz} and ϕ_{yz} respectively with ϕ_o denoting the power spectra associated with no devices in the jet nozzle or stilling section.

The first five Figures illustrate ϕ_{xz}, ϕ_{yz}, and ϕ_o for five different (r, θ) points of the radiative sound field associated with the airfoil type vortex generator. During these measurements, the angles of attack of the airfoils were maintained at $\pm$ 11.33 degrees. These Figures show that the vortex pair produces a definite asymmetry ($\phi_{xz} > \phi_{yz} > \phi_o$), in the far field spectra, relative to the z axis.

However, corresponding measurements, not shown here, made for the case of an exit Mach number of 0.9, show no detectable asymmetries in the far field spectra relative to the z axis.

In Figures 14 and 15, the increase in power spectral density with the magnitude of the angle of attack of the airfoils is depicted for a fixed far field (r, θ) point in the xz and yz planes respectively, These two Figures reveal an asymmetry, relative to the z axis, in the rate of increase of ϕ with the angle of attack α for the dimensionless frequency band $0.0242 \leq S \leq 0.0968$. The greatest increase in ϕ_{xz} comes in the range $0 \leq \alpha \leq 5.75$ while the greatest increase in ϕ_{yz} comes in the range $5.75 \leq \alpha \leq 11.33$.

Figures 16 to 18 illustrate ϕ_{xz} , ϕ_{yz} , and ϕ_o for three different (r, θ) points of the radiative sound field associated with the wing type turbulence generator. Here one finds a definite asymmetry in the power spectra only in the range $0.15 \leq S \leq .727$. It is to be noted also that this asymmetry, as far as the xz and yz planes are concerned, is the reverse of that associated in the power spectra due to the airfoil type vortex generator. In other words we have ($\phi_{yz} > \phi_{xz} > \phi_o$).

Since the asymmetries due to the vortex pair, produced by the airfoil type vortex generator, and the free stream turbulence, produced by the wing type turbulence generator, are opposite, one might expect mixed results for the case of asymmetries in the power spectra associated with the vane type vortex generator due to the fact that it produces both free stream turbulence and a vortex pair. This expectation is confirmed by Figures 19 to 22 which depict ϕ_{yz} , ϕ_{xz} , and ϕ_o for four different (r, θ)

points of the sound field associated with the vane type vortex generator. It is seen that in the region of space denoted by $r \geq 30$ inches an asymmetry in power spectra of the form ($\phi_0 \geq \phi_{yz} \geq \phi_{xz}$) exists while at r = 20 inches the reverse, relative to the xz and yz planes, is true.

Since the aforementioned mixed results fall into a definite pattern, relative to the distance from the origin of coordinates, one might be lead to believe that the non-radiative or pseudo sound field, whose pressure fluctuations satisfy the Laplace equation rather than a wave equation, had been extended from the domain $r \leq 15$ inches, associated with the absence of any device in the jet nozzle or the stilling section, to the domain $r \leq 20$ inches, due to the mixture of turbulence and large scale vorticity convected across the nozzle exit plane.

It is also to be noted that for both r = 20 inches and $r \geq 30$ inches most of the power spectra associated with the vane type device are less than that due to no device at all in the nozzle or stilling section. This is in contrast to the results due to the two preceeding devices.

If Figures 23, 24, and 25 are plotted ϕ_{xz} , ϕ_{yz} , and ϕ_0 for three different (r, θ) points of the far field associated with the cylinder type turbulence generator which produced a Karman vortex street with a frequency of vortex emission N equal to 3.0 Kc. Figures 26, 27, and 28 denote corresponding plots for a similar device with N = 5.7 Kc. The radiative sound field

associated with N = 3.0 Kc. has an asymmetry, in power spectra, relative to the z axis described by $\phi_{yz} > \phi_{xz} > \phi_o$ except at the point (30^o, 40^o), while that for N = 5.7 Kc. has, relative to the xz and yz planes, the reverse of this is true.

Except for the above change in asymmetry, which is small in magnitude, the power spectra, at corresponding points, for N = 3.0 Kc. and N = 5.7 Kc. are quite similar. This indicates that frequency of vortex emission, in the range $3.0 \leq N \leq 5.0$ Kc., is not overly critical in determining the average properties of the power spectral density of $\Delta p(\bar{r}, \bar{x})$ associated with the convection of a turbulent wake, containing a Karman vortex street, across the nozzle exit plane.

An analysis of Figures 23 to 28 also reveals that, in general, the temporal frequency at which ϕ_{xz} and ϕ_{yz} assume their peak value is greater by about 1.03 Kc. than that at which ϕ_o is maximized.

If the boundary layer, at the nozzle exit, is turbulent, then the power spectral density of the turbulent fluctuations, as stated in Section 2.2, will change its functional form as the turbulence is convected passed the point of transition in the free shear layer. If this is applied to the power spectra of the turbulent fluctuations of a turbulent wake, convected through the once laminar core into the free shear layer, with the realization that a change in functional form can mean a change in the maximizing frequency, then an explanation is possible in terms of shifts in the functional form of the power

spectra related to $\ddot{T}_{ij}$ causing shifts in the functional form of the far field spectra. In this case, the shift in functional from would be a change in the maximizing frequency, without gross distortion of the shape of the function.

In Figure 29 a comparison is made of ϕ_{xz} and ϕ_{yz} due to the airfoil and vane type vortex generators and wing type turbulence generator, for one (r, β) point in the far field, so as to give an idea of the relative changes in the power spectra induced by each device.

The greatest changes in power spectral density occur in the sound fields associated with the airfoil type vortex generator and the cylinder type turbulence generators where they increase by factors of 2.39 and 2.62 respectively.

5.3 The Filtered RMS Amplitudes

The rms averaged values of the radiative pressure fluctuation $\Delta p(\bar{r}, t)$ for energy associated with the temporal frequency range 0.5 Kc. to 15.0 Kc. are given below, in volts, for the radiative sound fields associated with the airfoil type vortex generator and the cylinder type turbulence generators. These values conform, in a comparative manner, with the plots of the power spectra given in Figs. 9 to 29. In the case of the vane type vortex generator and the wing type turbulence generator, the differences in power spectra for a given (r, β) point were so small that no difference in the rms amplitude of $\Delta p(\bar{r}, t)$ was measureable.

AIRFOIL TYPE VORTEX GENERATORS

r in inches	β	xz plane	yz plane	no device used	filtered rms voltage
30	20^{o}	x			2.35
30	20^{o}		x		2.25
30	20^{o}			x	2.25
36	30^{o}	x			1.72
36	30^{o}		x		1.70
36	30^{o}			x	1.70
20	20^{o}	x			1.20
20	20^{o}		x		1.18
20	20^{o}			x	1.16
20	30^{o}	x			1.05
20	30^{o}		x		1.03
20	30^{o}			x	1.03
20	40^{o}	x			0.76
20	40^{o}		x		0.75
20	40^{o}			x	0.74

CYLINDER TYPE TURBULENCE GENERATORS

r in inches	β	N in Kc.	xz plane	yz plane	no device used	filtered rms voltage
30	25°	3.0	x			3.2
30	25°	3.0		x		3.2
30	25°	3.0			x	2.4
30	30°	3.0	x			3.1
30	30°	3.0		x		3.1
30	30°	3.0			x	2.25
30	40°	3.0	x			2.5
30	40°	3.0		x		2.4
30	40°	3.0			x	1.6
30	25°	5.7	x			3.2
30	25°	5.7		x		3.2
30	25°	5.7			x	2.4
30	30°	5.7	x			3.0
30	30°	5.7		x		3.0
30	30°	5.7			x	2.25
30	40°	5.7	x			2.4
30	40°	5.7		x		2.4
30	40°	5.7			x	1.6

CHAPTER 6

CONCLUSION

The measurements of the rms amplitude and power spectral density of the radiative pressure fluctuation, described in Chapter 5, indicate that small changes in the mean velocity field and the introduction of a turbulent velocity field at the nozzle exit plane cause definite changes to occur in the structure of the radiative sound field.

This is illustrated by the fact that a vortex pair, inducing a maximum velocity of magnitude 3.52 feet/second and with direction perpendicular to the z axis at the nozzle exit plane, can cause the peak value of power spectral density to become, at some points, 2.39 times its original value. In the case of turbulent wakes, each containing a Karman vortex street, with vortex emission frequencies of 3.0 Kc. and 5.7 Kc., convected across the nozzle exit plane the above factor can be increased to 2.62. The resul ts for the two values of emission frequency were quite similar.

The changes in the structure of the radiative sound field also exhibit themselves in terms of asymmetries, relative to the

z axis, in the rms amplitude and power spectral density of the radiative pressure fluctuation. It is also to be noted that the asymmetries associated with a vortex pair at the nozzle exit plane are opposite, in general, to those associated with free stream turbulence, without Karman vortex street, convected across the nozzle exit plane.

Of interest, in the area of applications to the reduction of jet engine noise, is the fact that in contrast to the cases of relatively pure vortex pair and free stream turbulence, a mixture of the two will cause the power spectral density to decrease farther than increase. While the maximum factor of reduction is only 0.853, the helix angle, directly associated with jet engine thrust reduction, is also quite small (0.15^{o}). Such results recommend the design of devices, similar to the vane type vortex generator, which would increase the helix angle to say 1.5^{o} , which would still involve a negligible decrease in thrust but would cause a greater decrease in the power spectral density at some points in the far field.

While not directly relevant to jet engine noise reduction applications, the 1.03 Kc. shift in the maximizing frequency of the power spectra associated with the cylinder type turbulence generators is of theoretical interest in that it may, if augmented by further work in this area, give some idea as to the finer details of the sound production process. It is felt that this further work should include measurements of the power spectral density of the turbulent fluctuations in turbulent

wakes before and after they are convected past the point of transition in the free shear layer. Such spectra could then be compared with the corresponding spectra associated with the turbulent fluctuations in a turbulent boundary layer at the nozzle exit, and, of course, with the corresponding radiative sound field spectra in each case.

REFERENCES

1. Batchelor, G.K., The Theory of Homogeneous Turbulence, Cambridge University Press, 1960.

2. Burgers, J.M., The Effect of Stretching of a Vortex Core, University of Maryland, Institute for Fluid Mechanics and Applied Mathematics, Technical Note, BN-80, 1956.

3. Hinze, J.O., Turbulence, McGraw-Hill Book Company, Inc., 1959.

4. Kolpin, M.A., Flow in the Mixing Region of a Jet, ASRL TR 92-3, Massachusetts Institute of Technology, 1962.

5. Lighthill, M.J., On Sound Generated Aerodynamically, Part 1 - General Theory, Proc. Roy. Soc. of London, Vol. 211, pp. 564-587, 1952.

6. Lighthill, M.J., On Sound Generated Aerodynamically, Part 2 - Turbulence as a Source of Sound, Proc. Roy. Soc. of London, Vol. 222, pp. 1-32, 1954.

7. Lighthill, M.J., Sound Generated Aerodynamically, The Bakerian Lecture, Royal Aircraft Establishment, Tech. Memo, December 8, 1961.

8. Lighthill, M.J., Jet Noise, The Wright Brothers Memorial Lecture, Royal Aircraft Establishment, Tech. Memo., December 17, 1963.

9. Milne-Thomson, L.M., Theoretical Hydrodynamics, The MacMillan Company, 1950.

10. Mollo-Christensen, E.L., Kolpin, M.A., and Martuccelli, J.R., Experiments on Jet Flows and Jet Noise Far Field Spectra and Directivity Patterns, ASRL TR 1007, Massachusetts Institute of Technology, 1963.

11. Richardson, E.G., Dynamics of Real Fluids, Edward Arnold and Company, 1950.

12. Townsend, A.A., The Structure of Turbulent Shear Flow, Cambridge University Press, 1956.

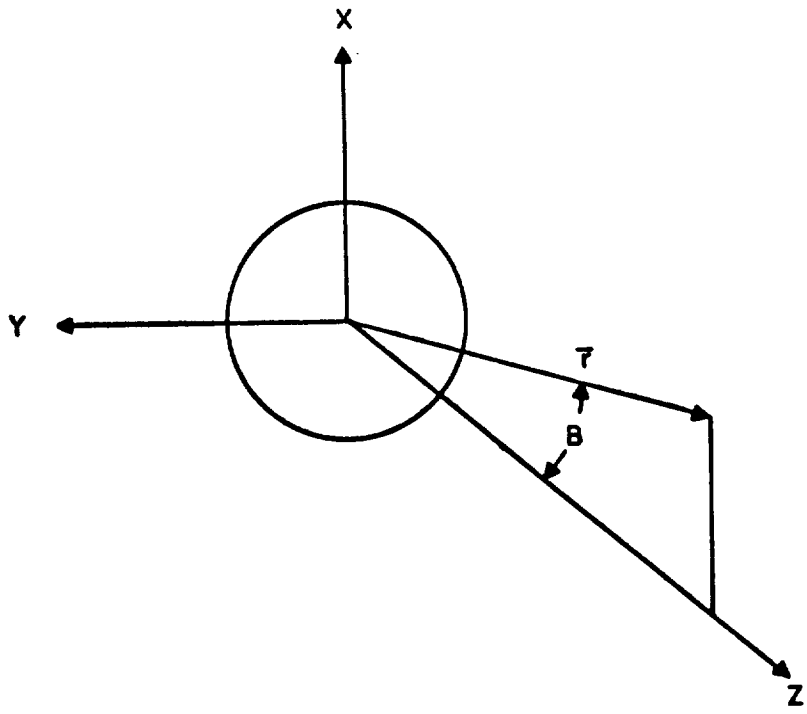

Figure 1 Coord. System for Describing Far Field

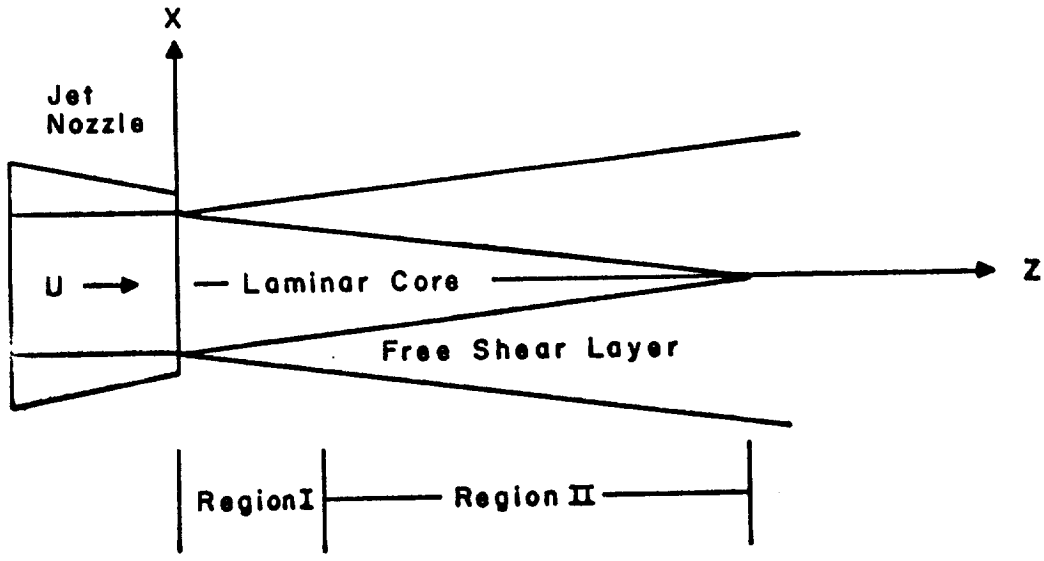

Figure 2 Cross Section Diagram of Jet

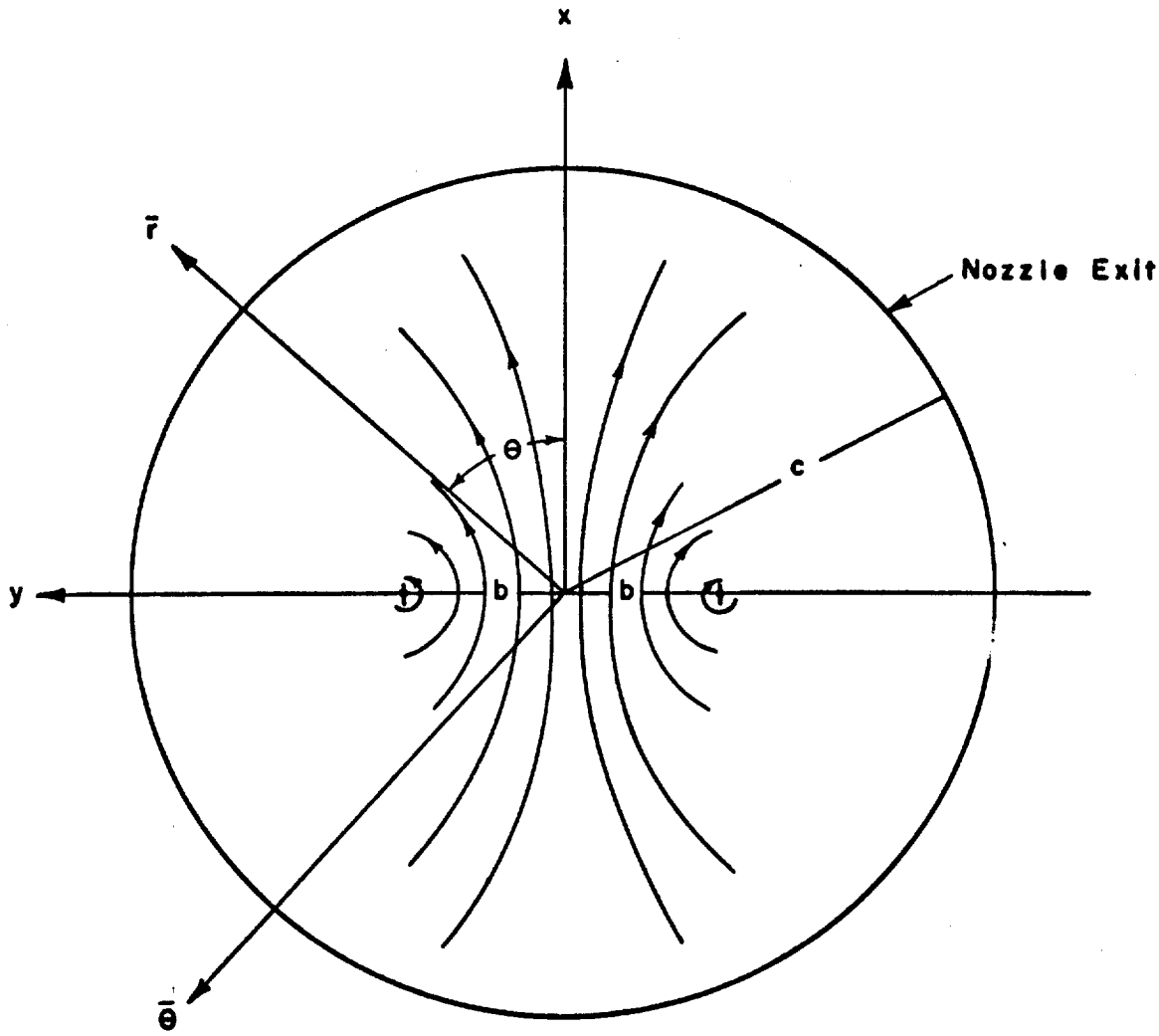

Figure 3 Geometry of Vortex Pair at the Nozzle Exit Plane

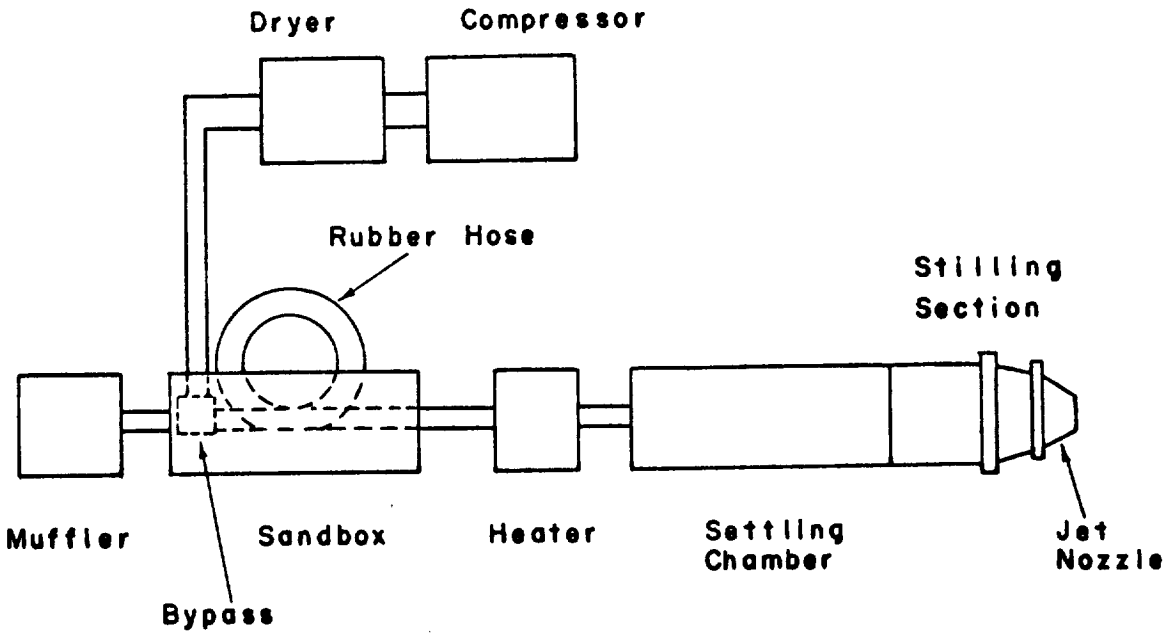

Detail of Flow Producing Apparatus

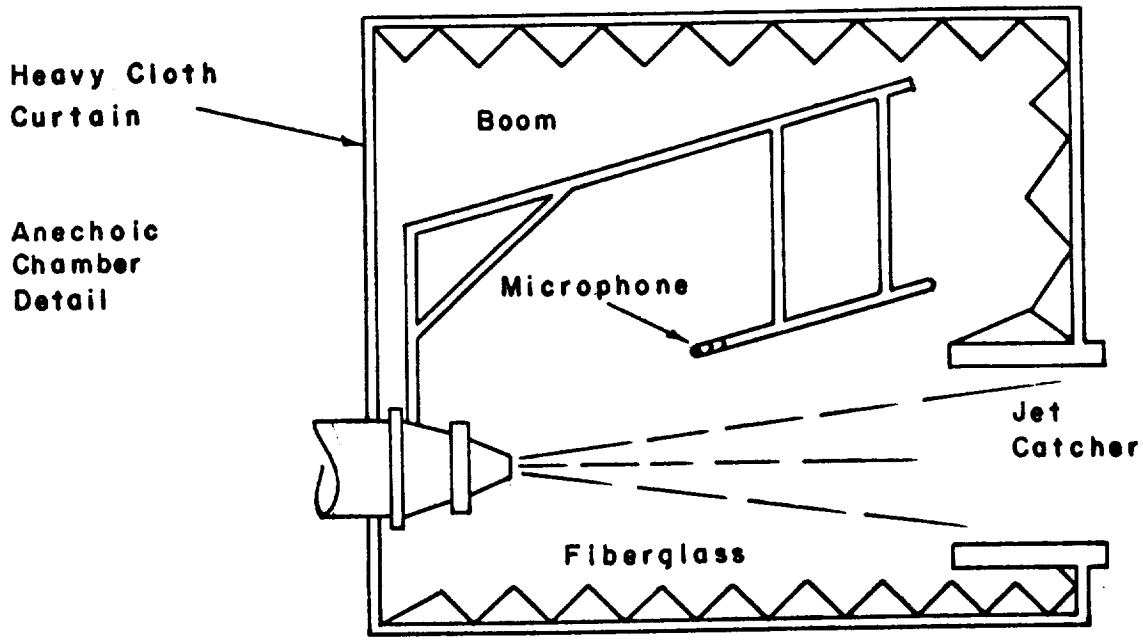

Figure 4 Flow Apparatus

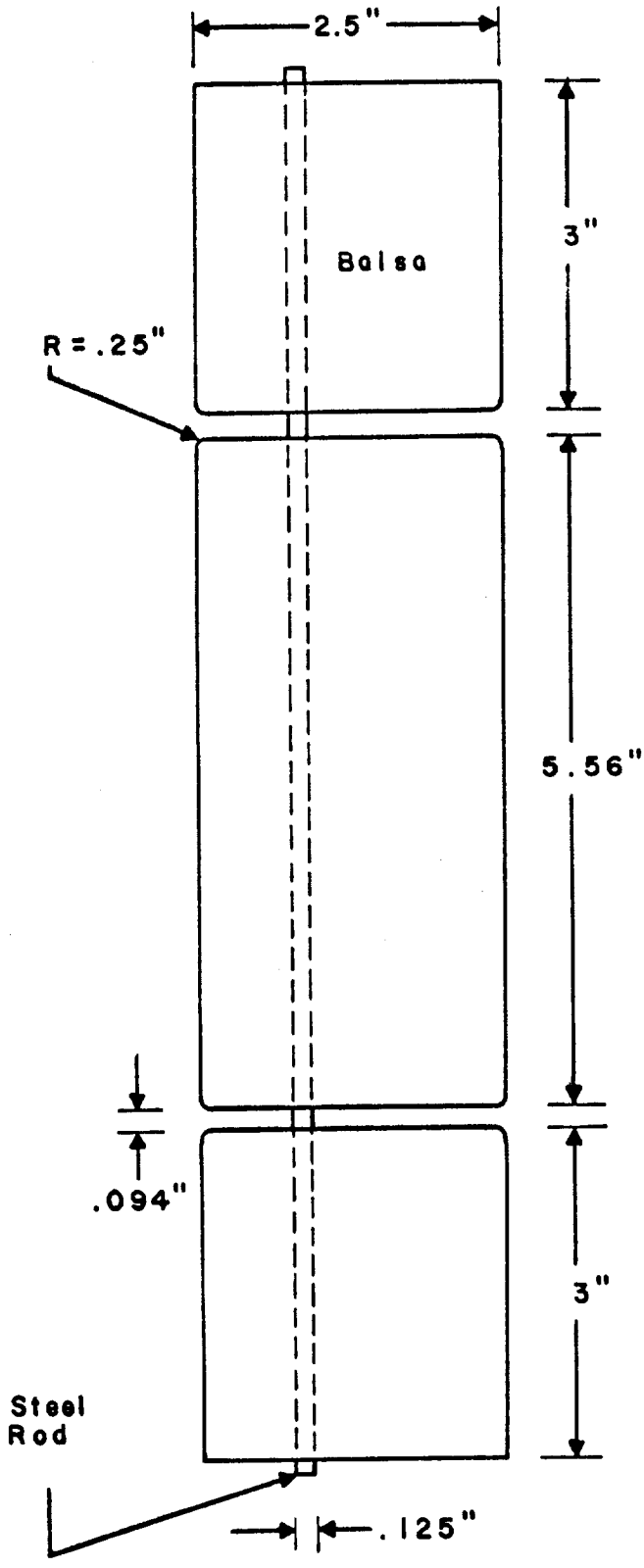

Figure 5 Airfoil Type Vortex Generator

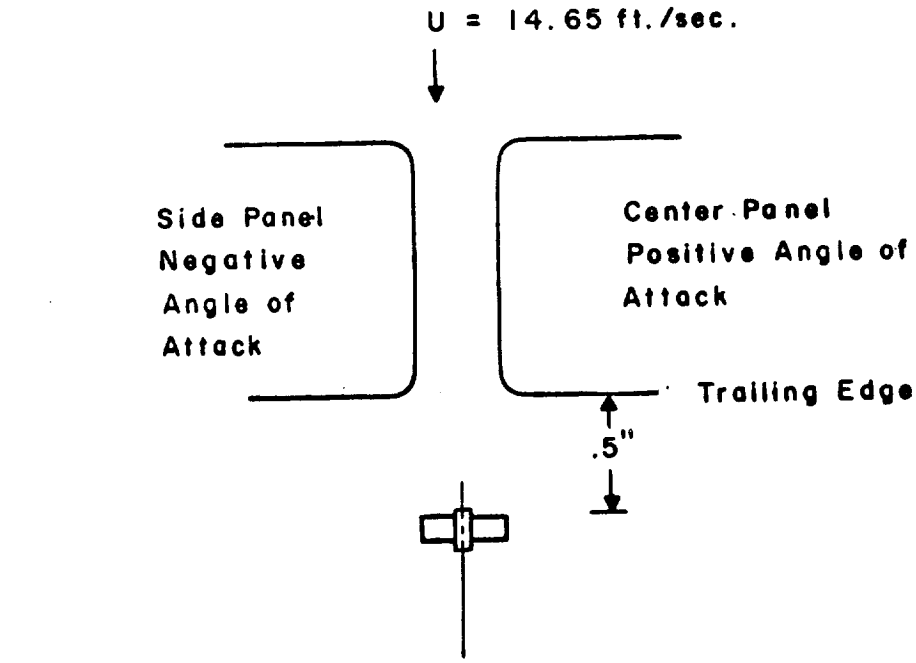

Vortometer Mounting Detail

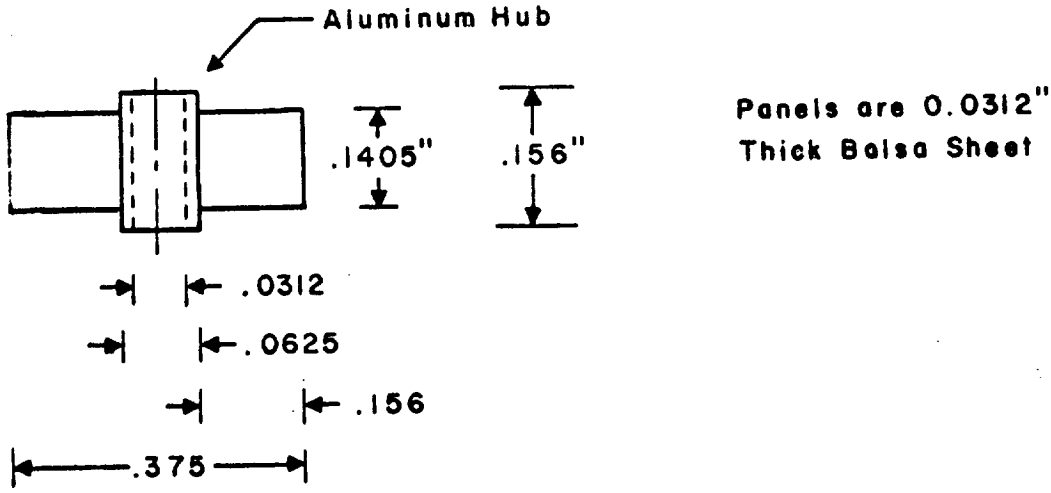

Vortometer Detail

Figure 6 Apparatus Used in Measurement of Angluar Velocity of the Rigid Body Core

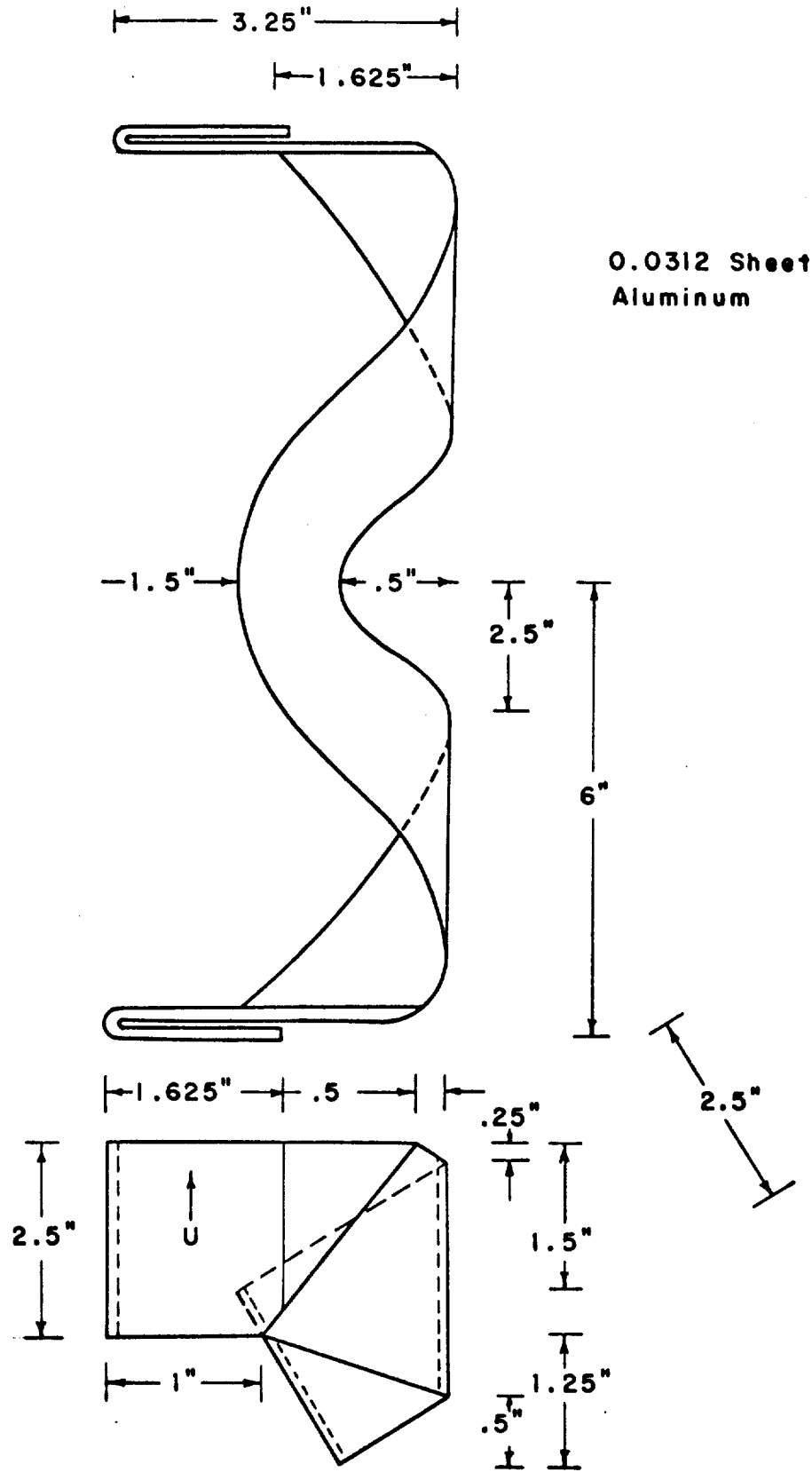

Figure 7 The Vane Type Vortex Generator

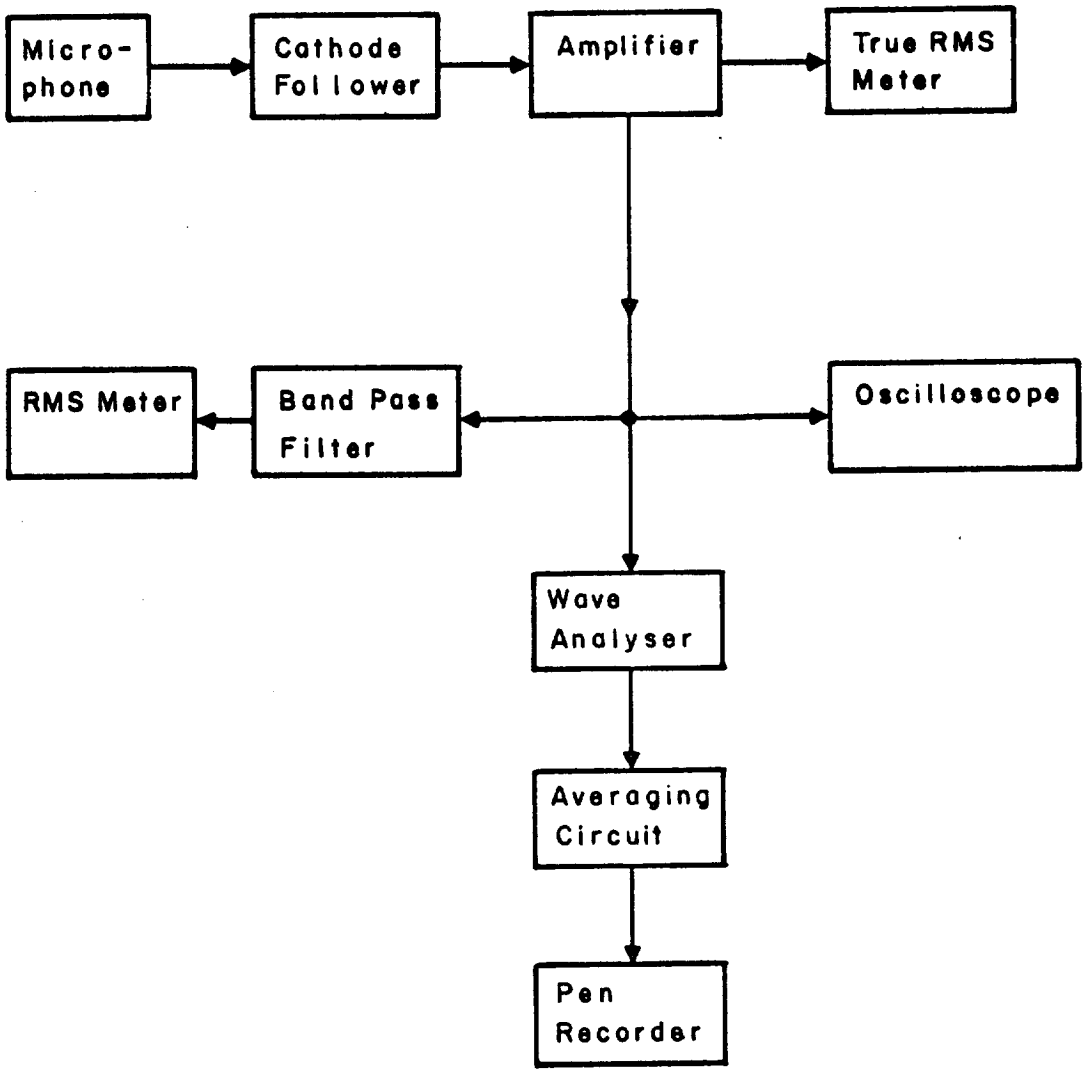

Figure 8 Signal Processing System

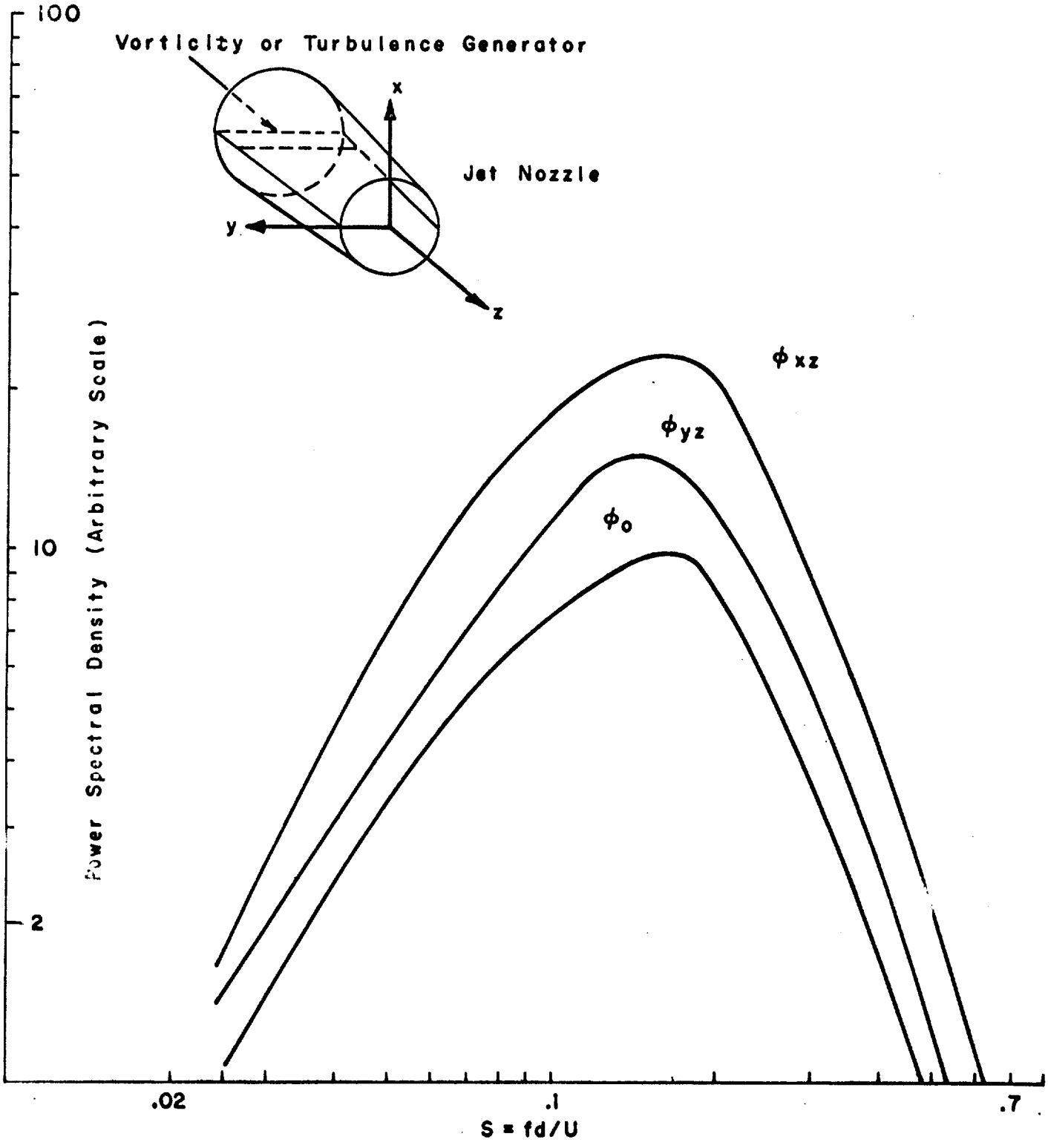

Figure 9 Far Field Spectra Associated With Airfoil Type Vortex Generator $r = 30''$, $\beta = 20°$

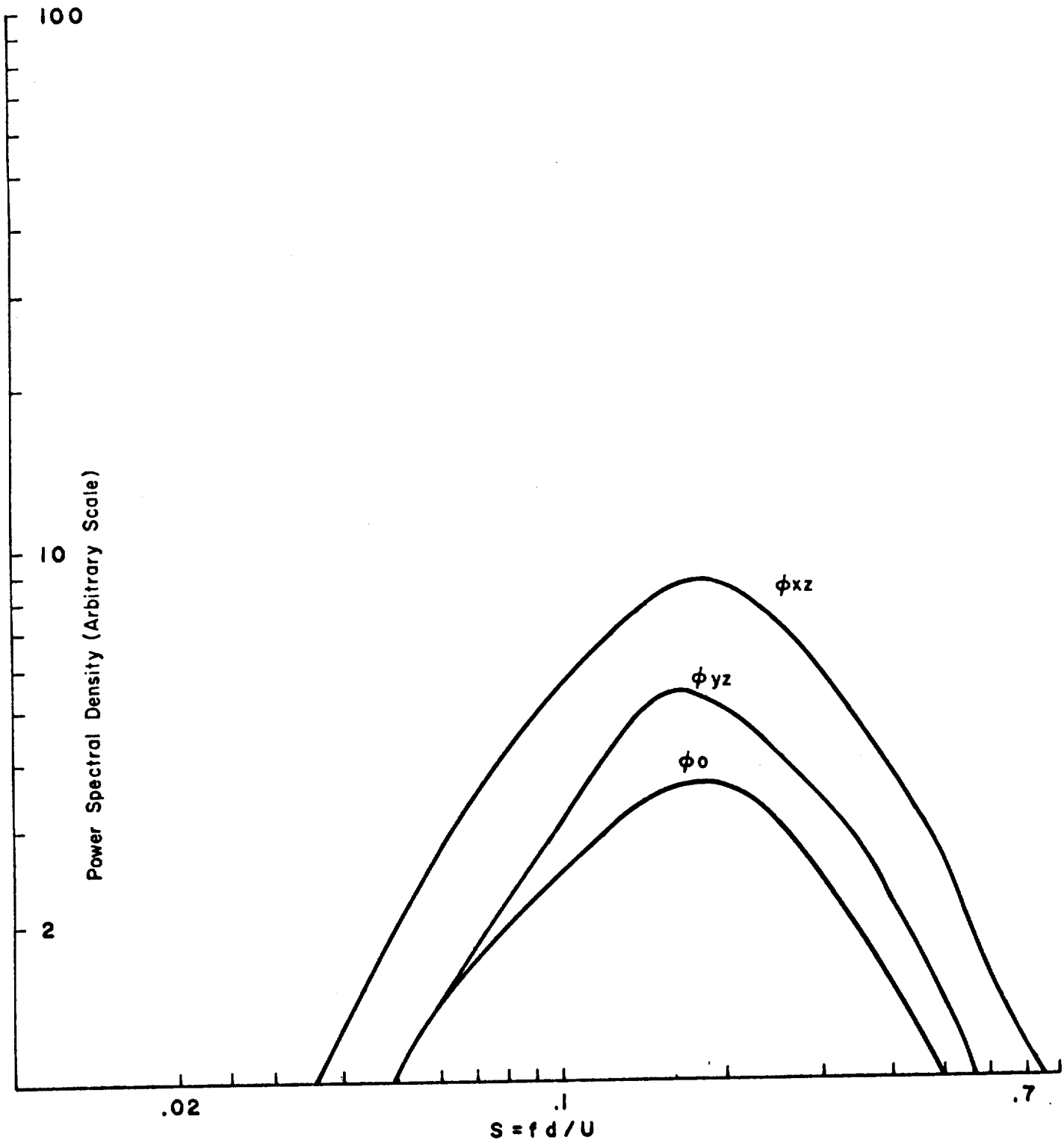

Figure 10 Far Field Spectra Associated With Airfoil Type Vortex Generator $r = 36''$, $\beta = 30°$

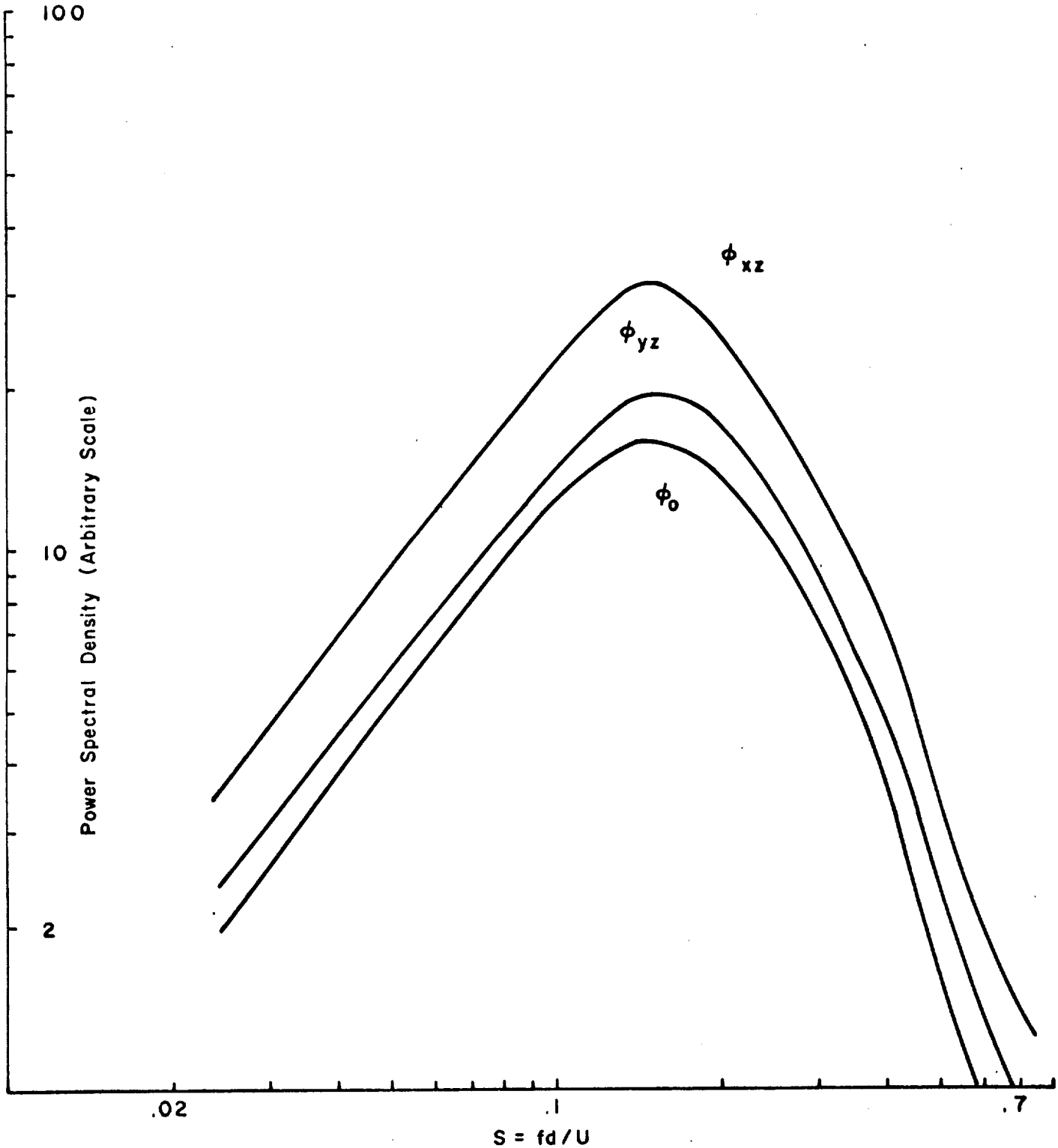

Figure 11 Far Field Spectra Associated With Airfoil Type Vortex Generator
$r = 20''$, $\beta = 20°$

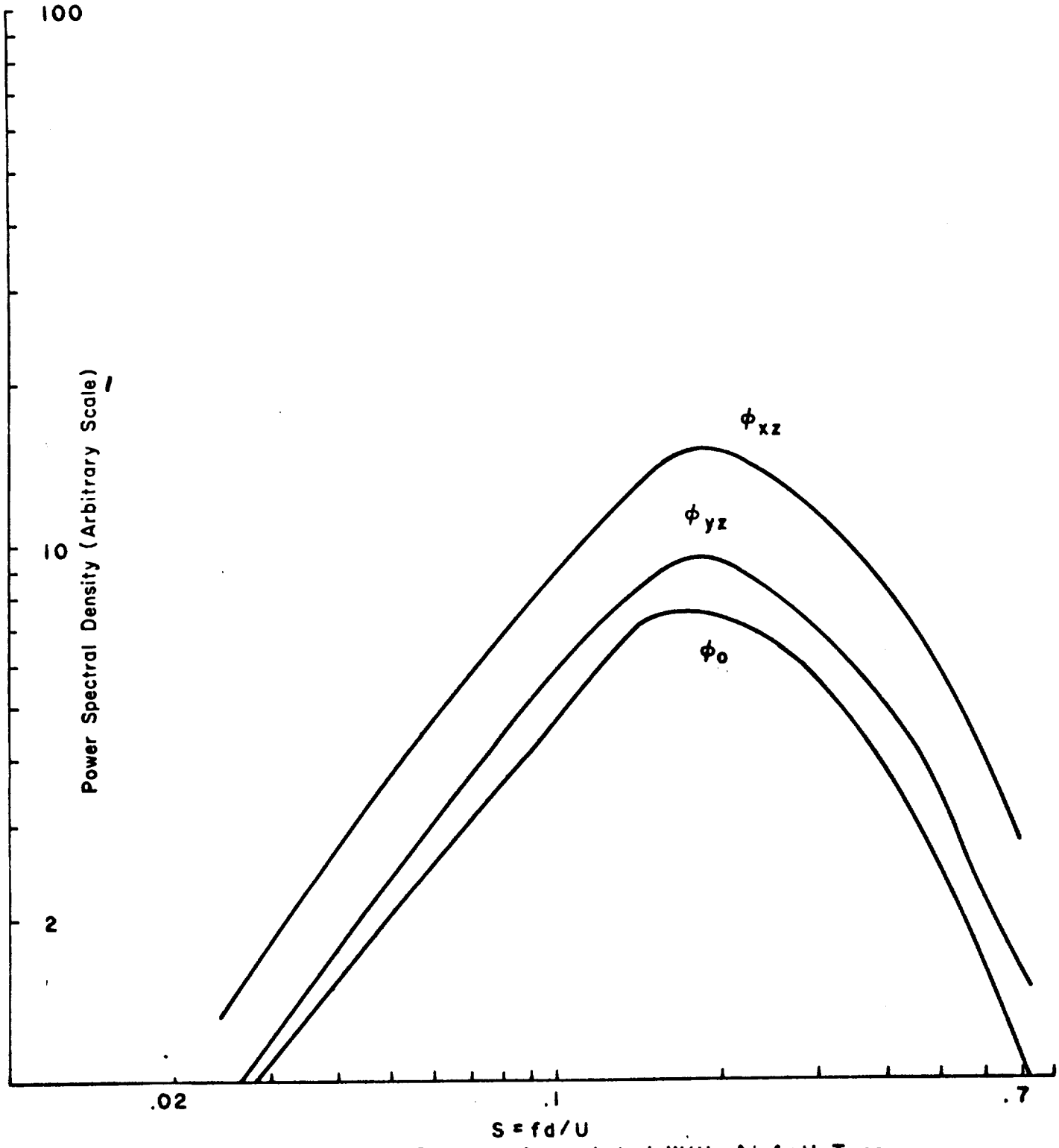

Figure 12 Far Field Spectra Associated With Airfoil Type Vortex Generator
r = 20", β = 30°

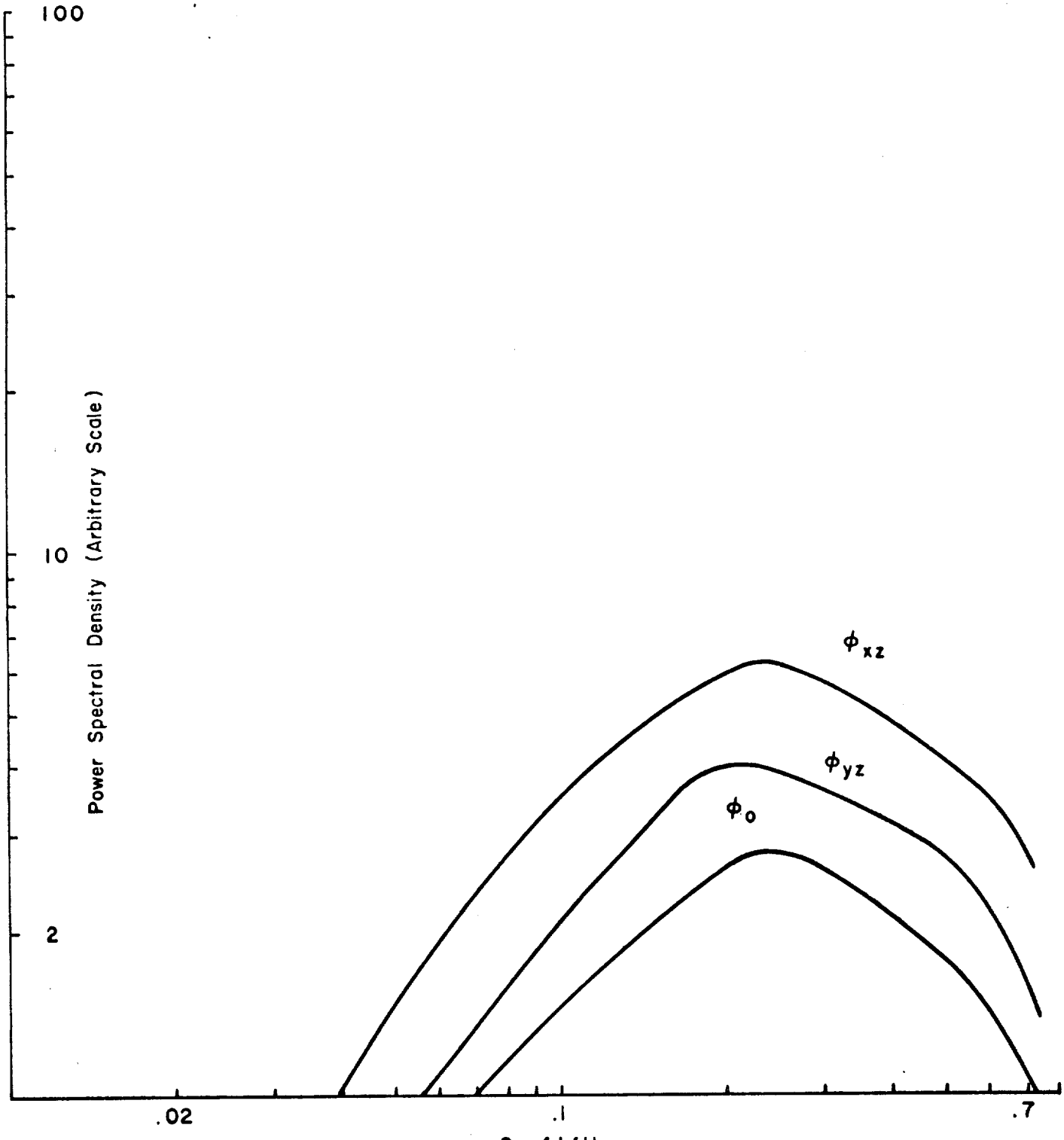

Figure 13 Far Field Spectra Associated With Airfoil Type Vortex Generator
r = 20", β = 40°

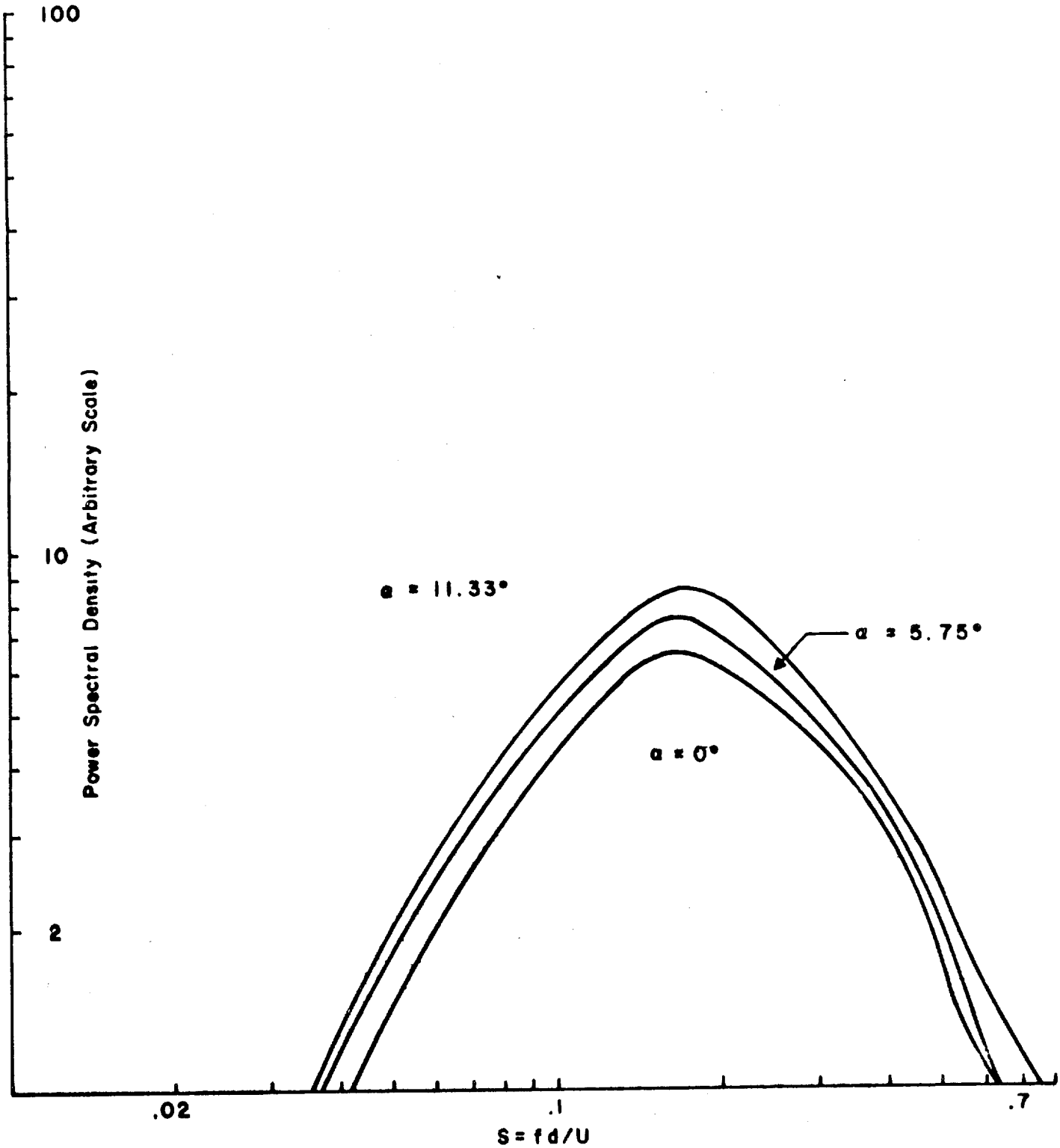

Figure 14 Variation of Far Field Spectra With Angle of Attack of Airfoil Type Vortex Generator in XZ Plane r = 36", $\beta = 30°$

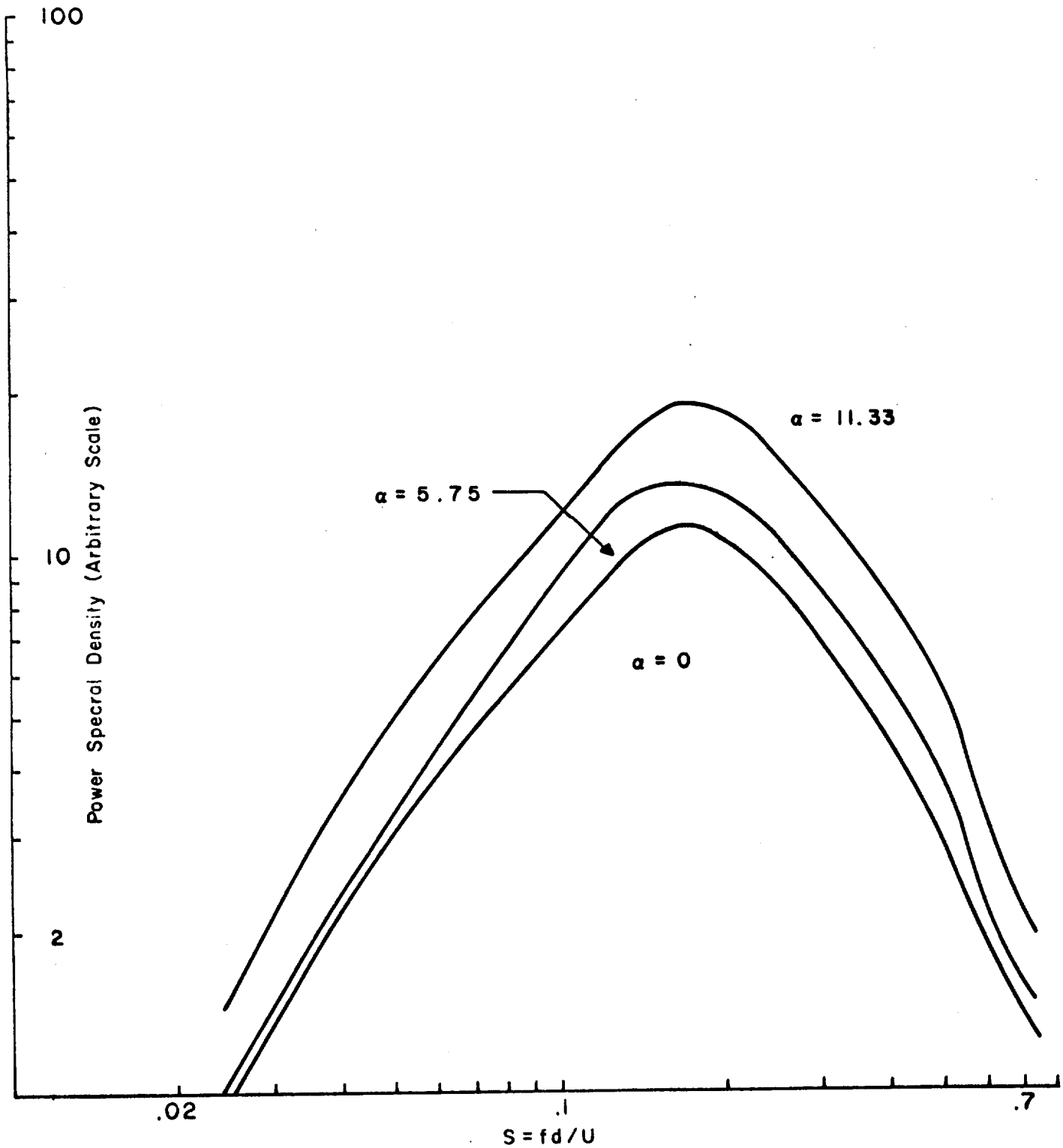

Figure 15 Variation of Far Field Spectra With Angle of Attack of Airfoil Type Vortex Generator In XZ Plane
r = 36", β = 30°

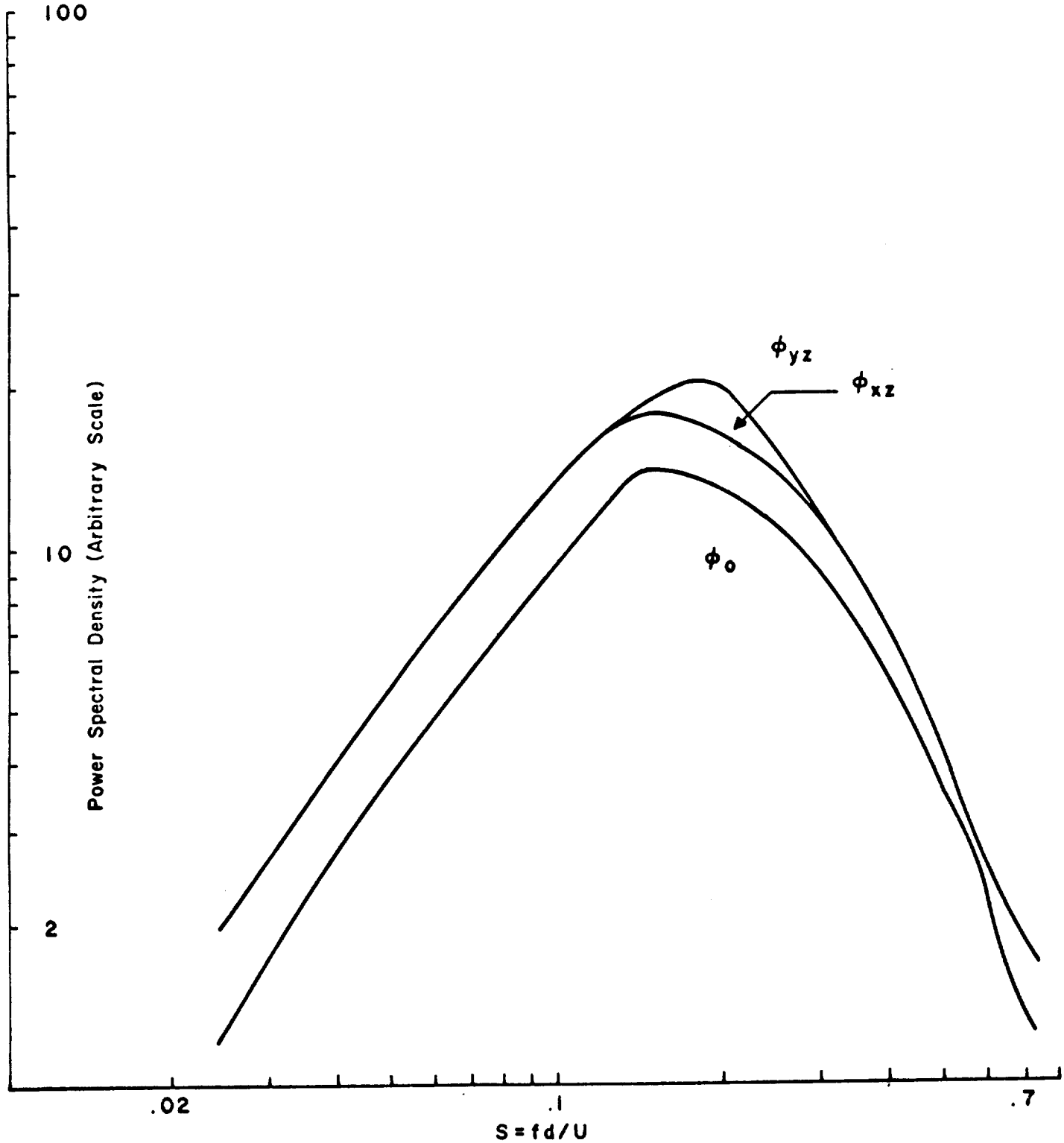

Figure 16 Far Field Spectra Associated With Wing Type Turbulence Generator
r = 36", β = 30°

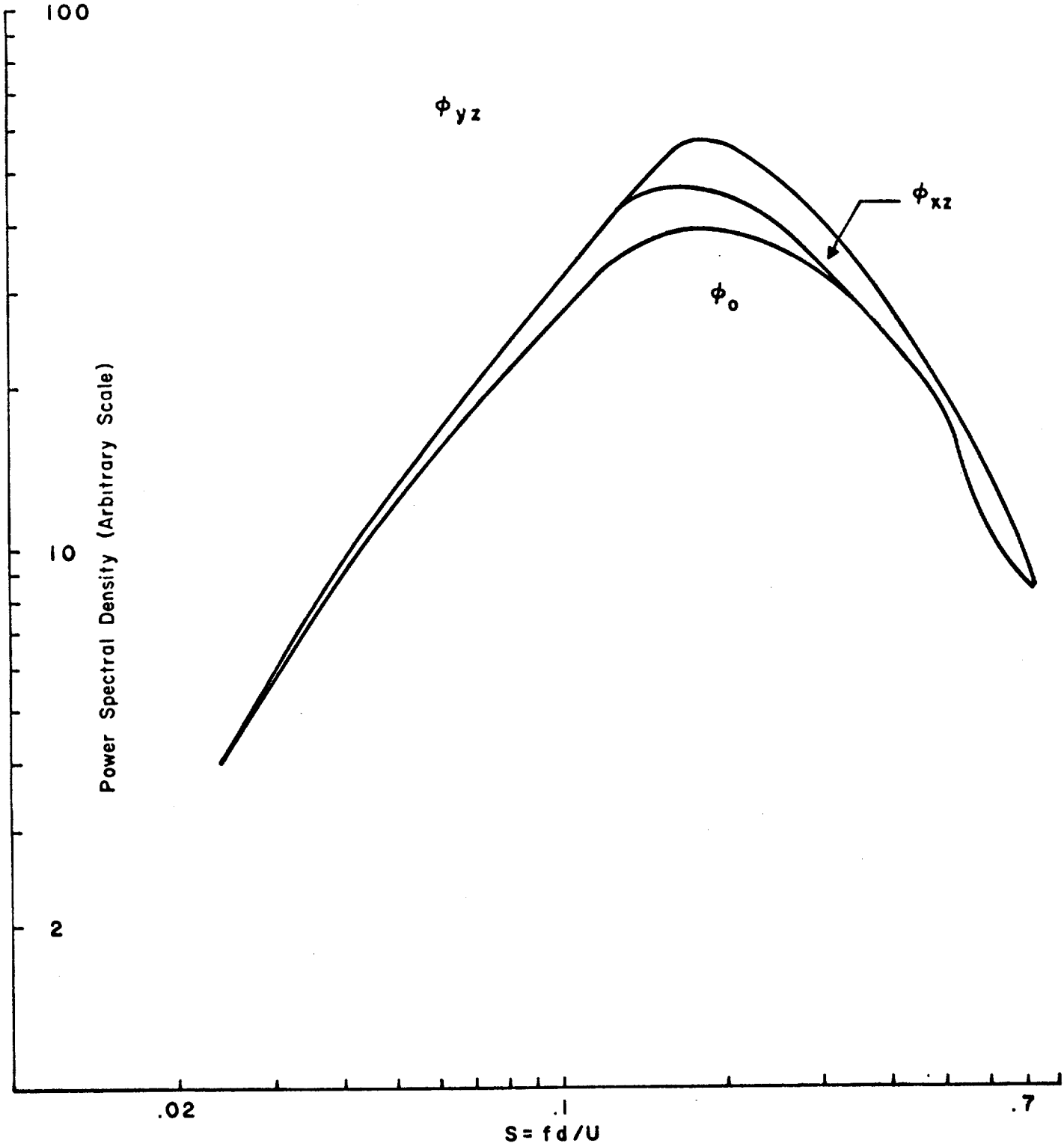

Figure 17 Far Field Spectra Associated With Wing Type Turbulence Generator
$r = 20''$, $\beta = 30°$

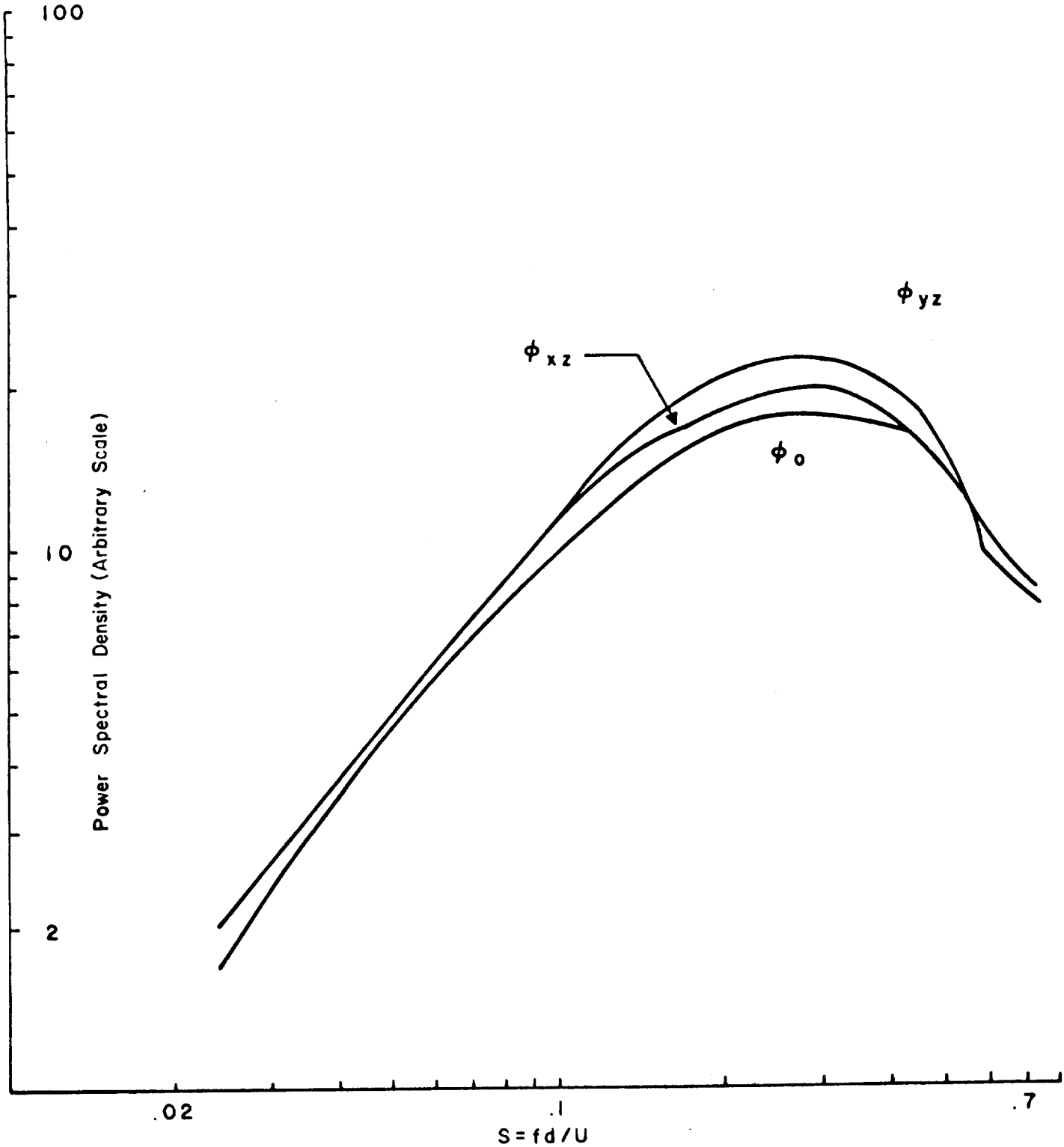

Figure 18 Far Field Spectra Associated With Wing Type Turbulence Generator

$r = 20''$, $\beta = 40°$

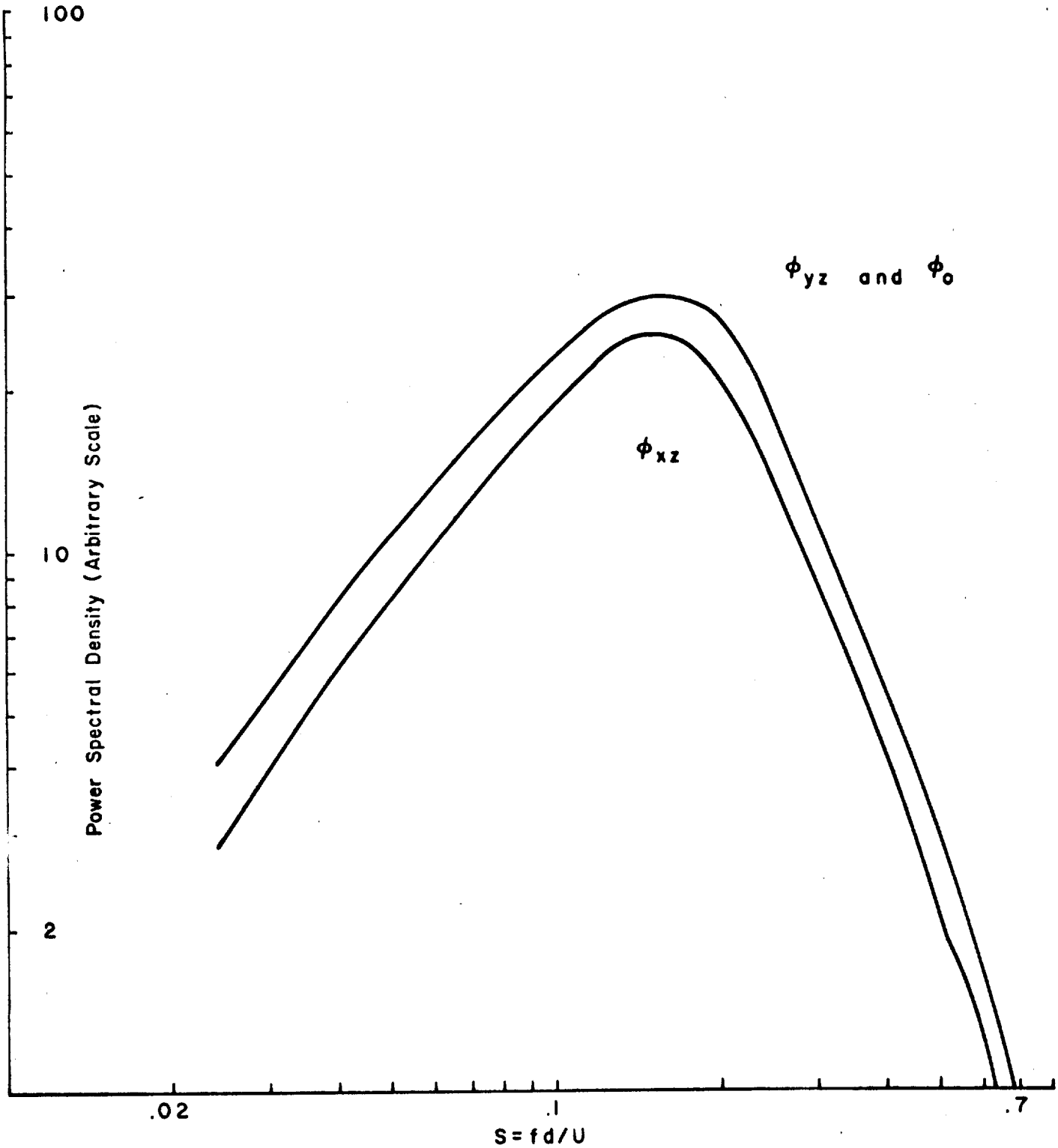

Figure 19 Far Field Spectra Associated With Vane Type Vortex Generator

$r = 30''$, $\beta = 20°$

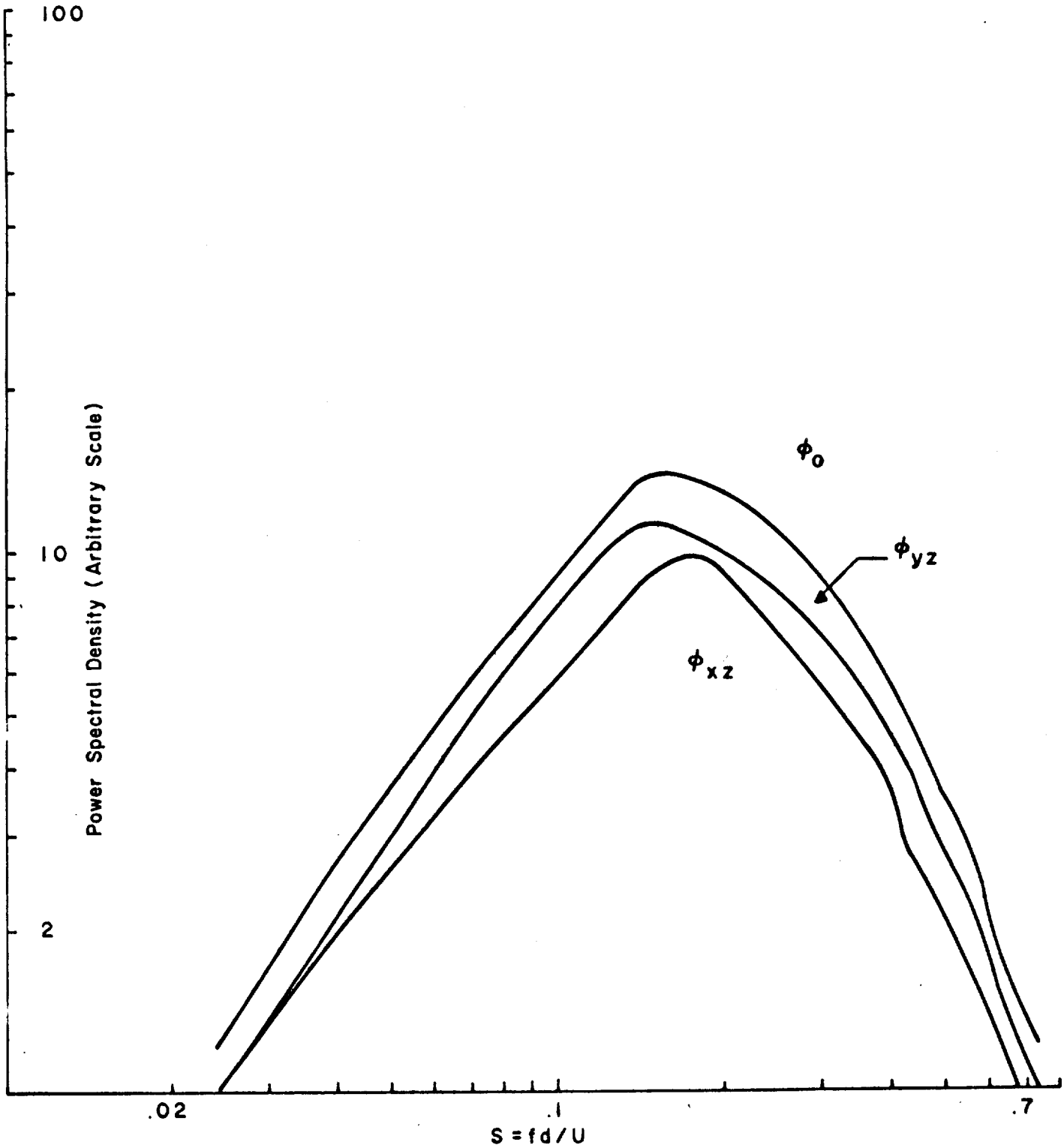

Figure 20 Far Field Spectra Associated With Vane Type Vortex Generator
$r = 36"$, $\beta = 30°$

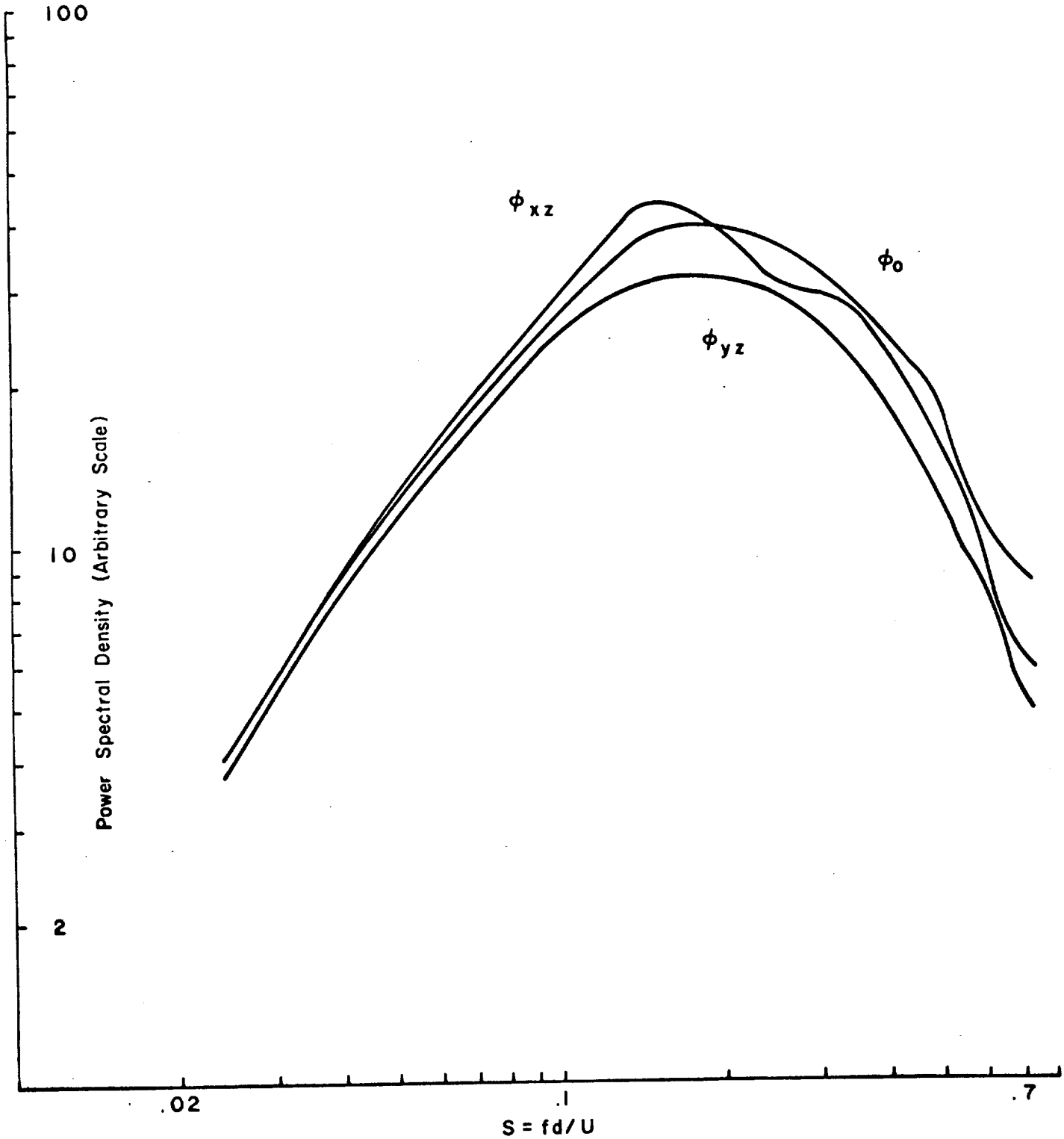

Figure 21 Far Field Spectra Associated With Vane Type Vortex Generator

$r = 20''$, $\beta = 30°$

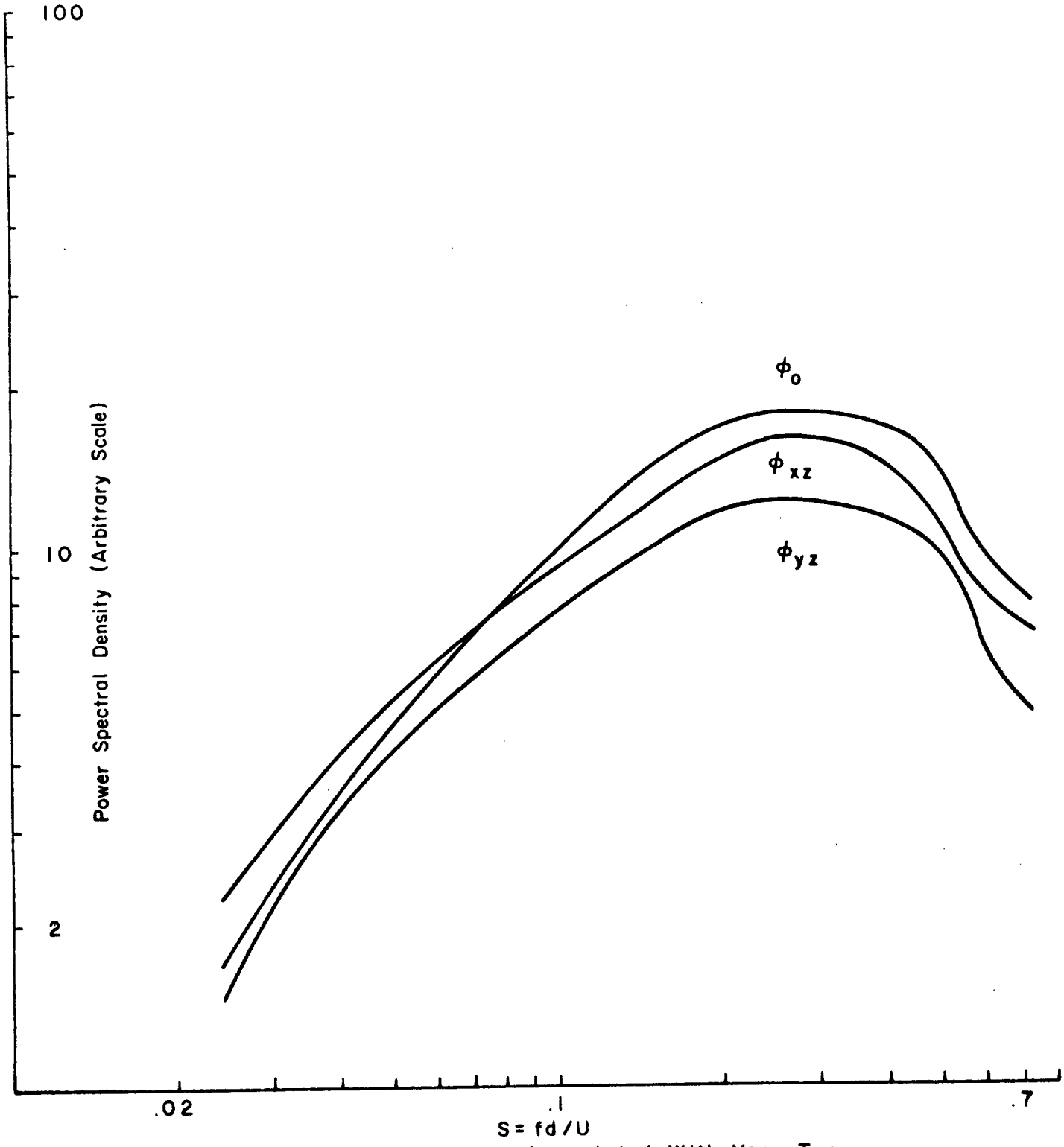

Figure 22 Far Field Spectra Associated With Vane Type Vortex Generator
r = 20", β = 40°

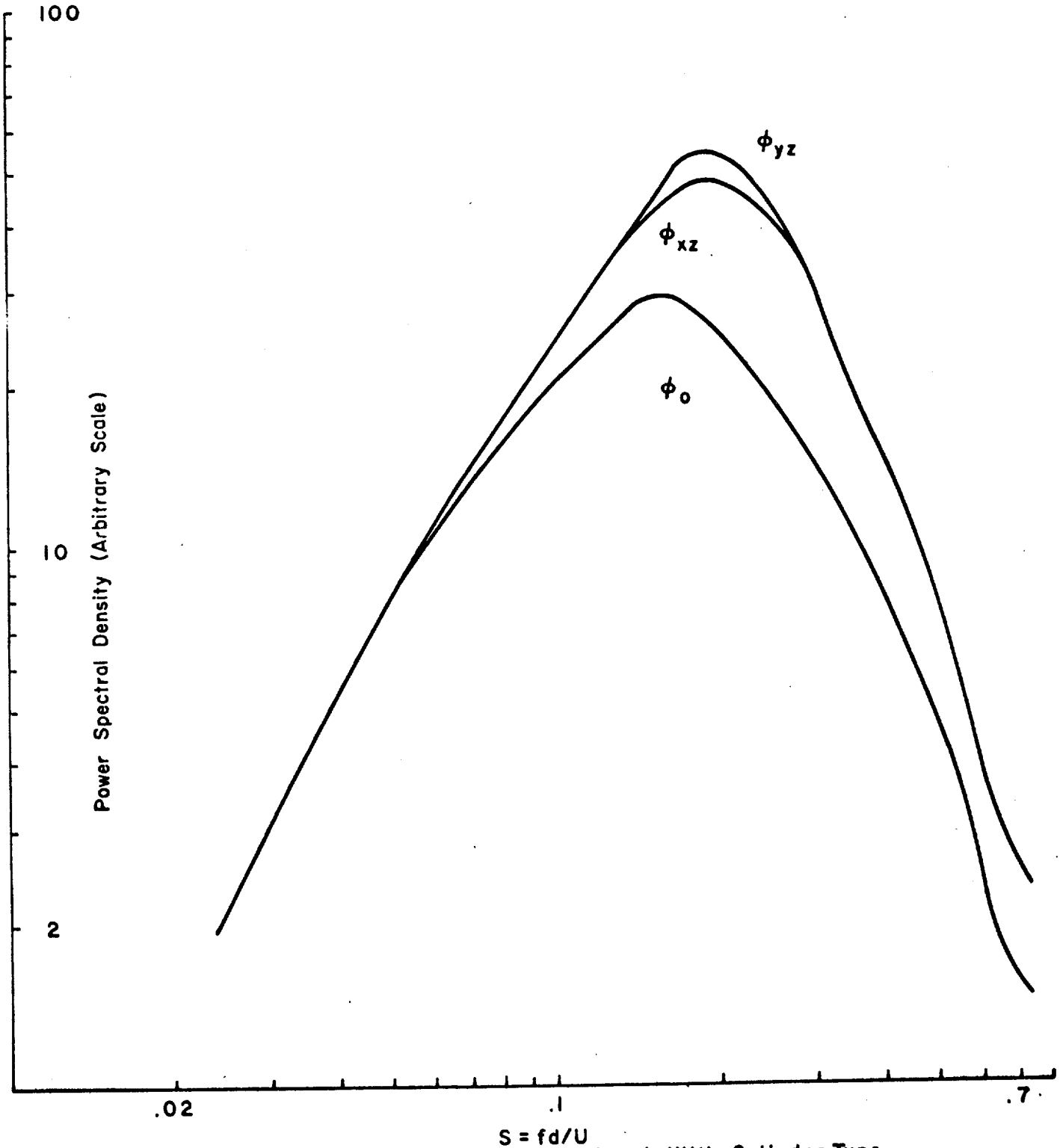

Figure 23 Far Field Spectra Associated With Cylinder Type Turbulence Generator

N = 3.0 Kc.

r = 30", β = 25°

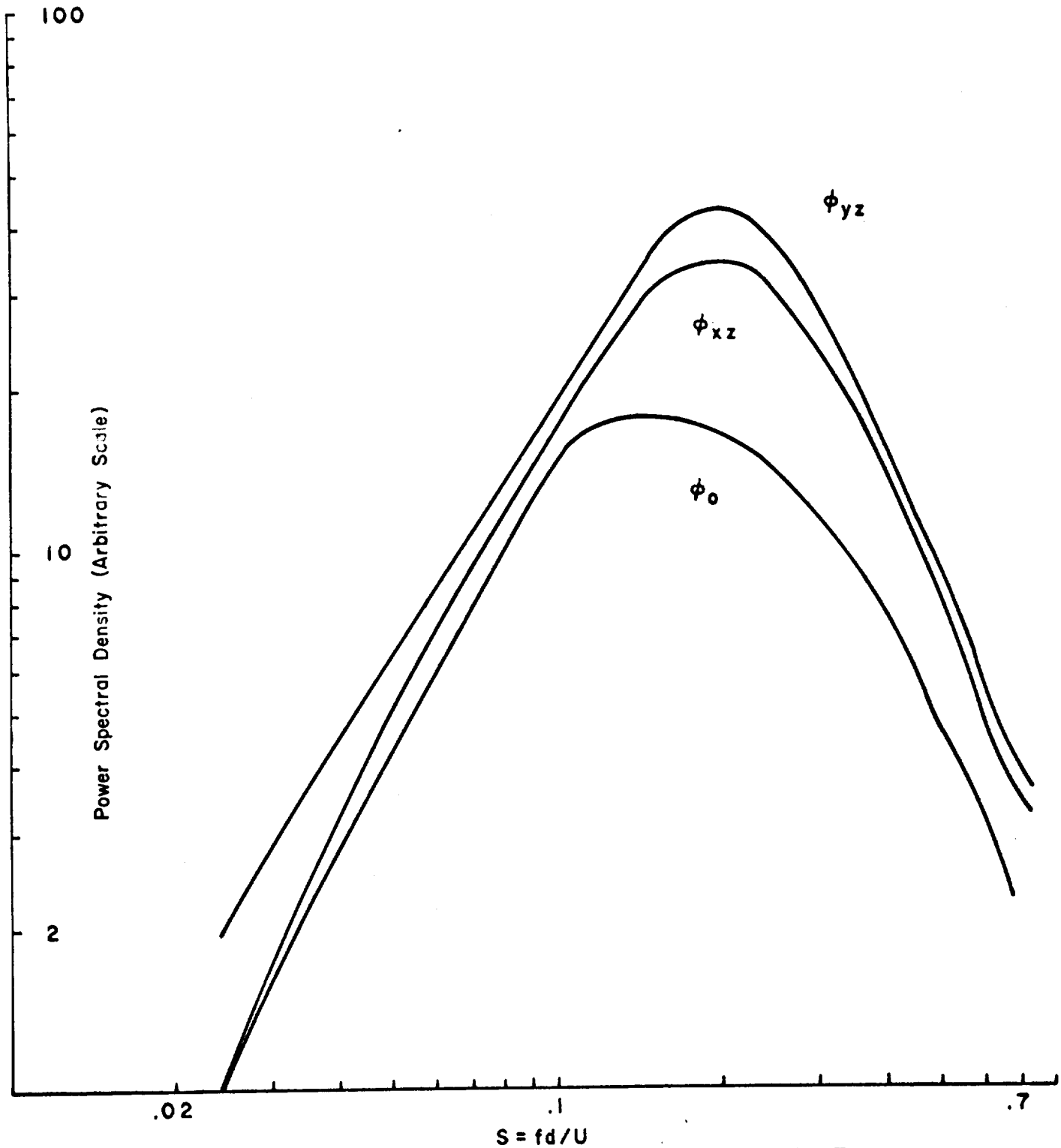

Figure 24 Far Field Spectra Associated With Cylinder Type Turbulence Generator

N = 3.0 Kc.

r = 30", β = 30°

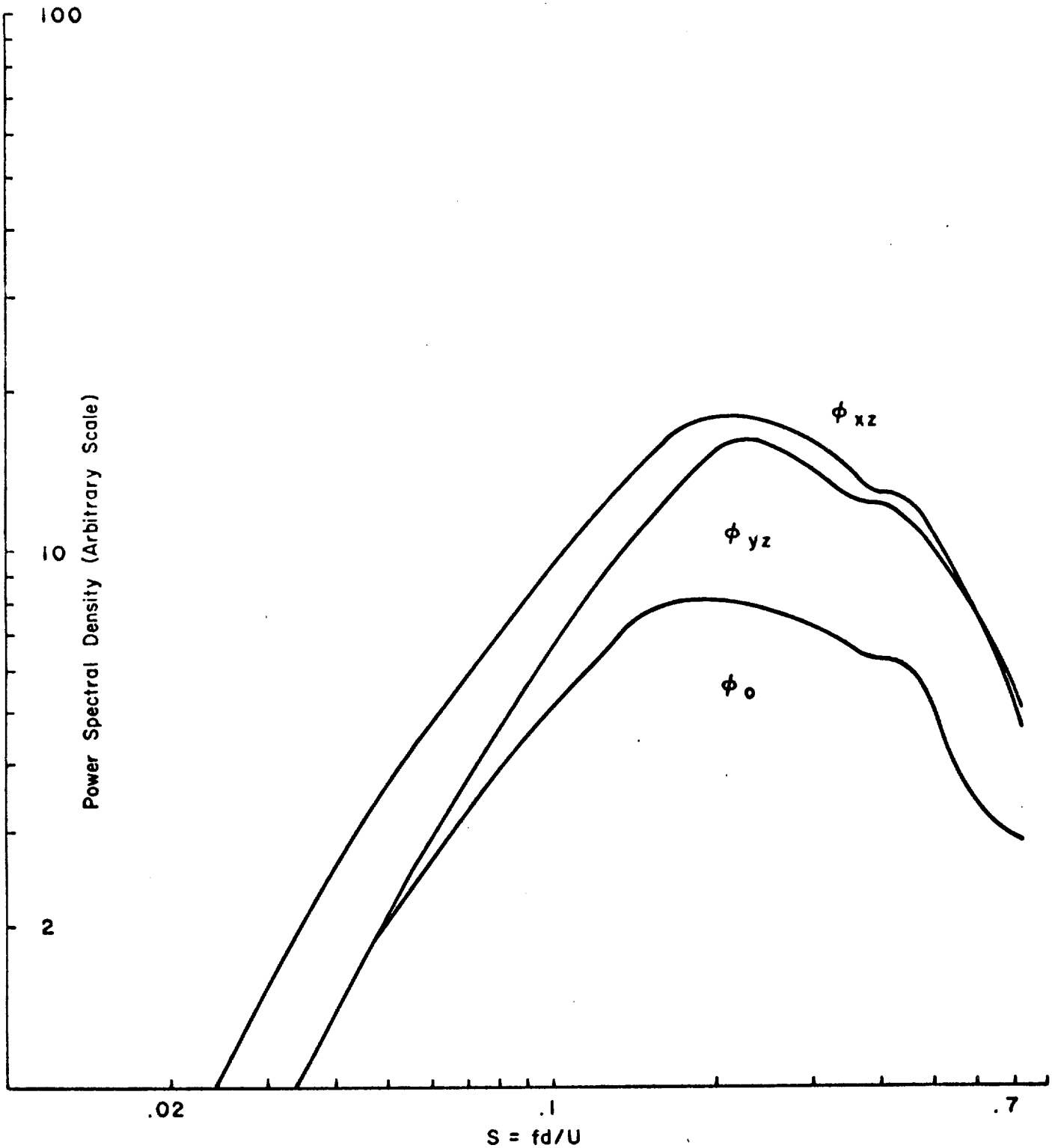

Figure 25 Far Field Spectra Associated With Cylinder Type Turbulence Generator

N = 3.0 Kc.
r = 30", β= 40°

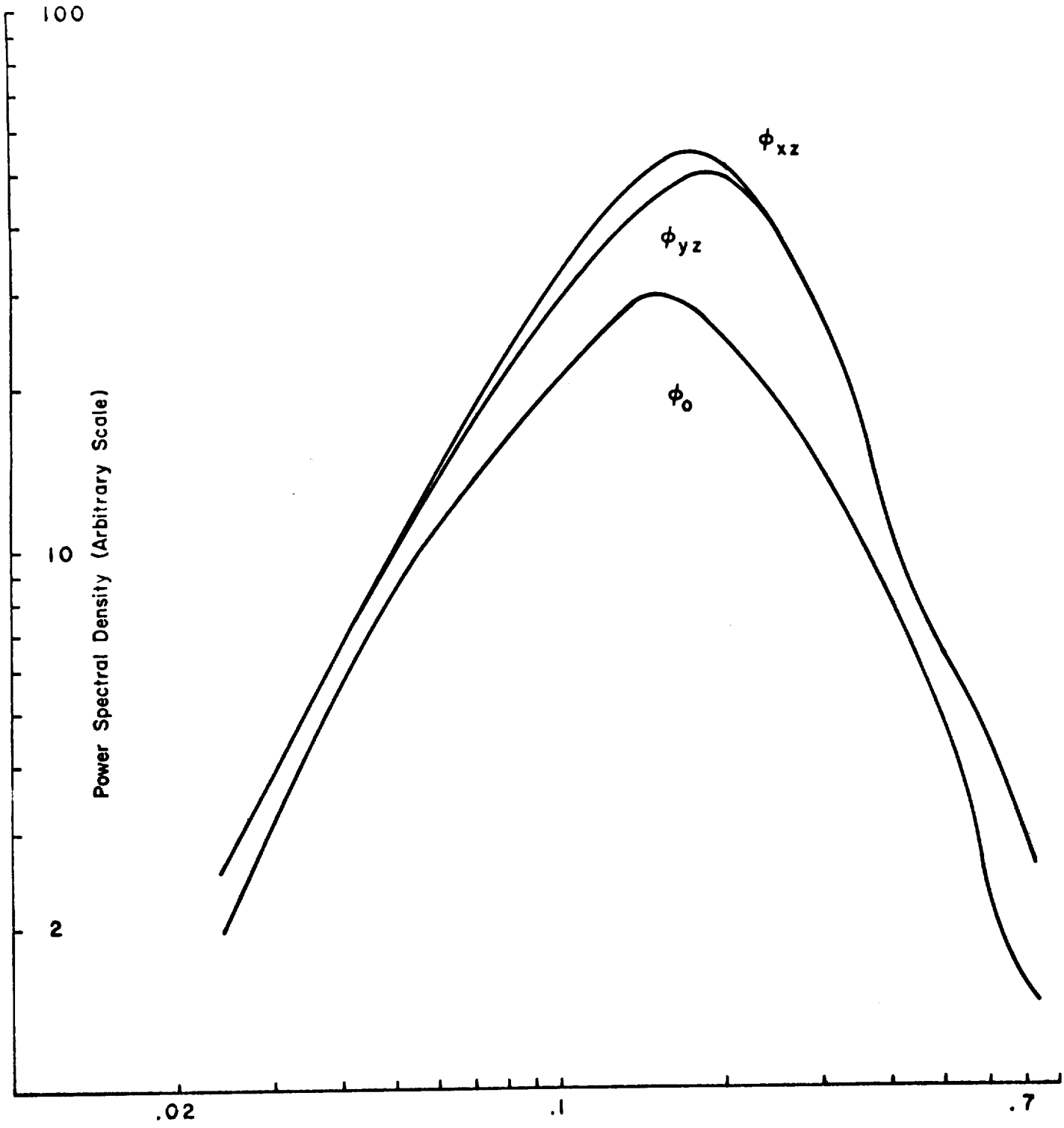

Figure 26 Far Field Spectra Associated With Cylinder Type Turbulence Generator

N = 5.7 Kc.

r = 30", β = 90°

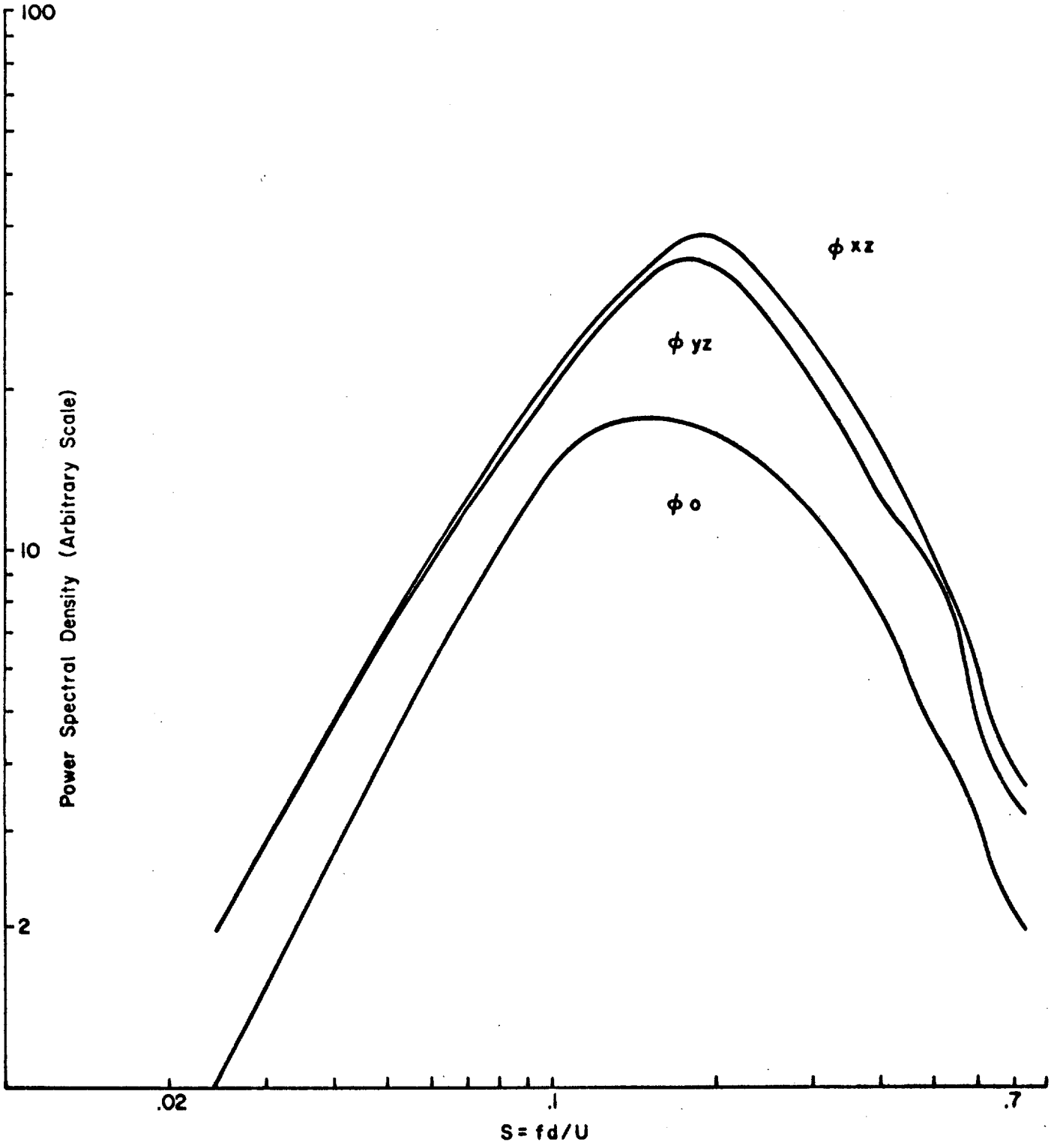

Figure 27 Far Field Spectra Associated With Cylinder Type Turbulence Generator N = 5.7 Kc. r = 30", β = 30°

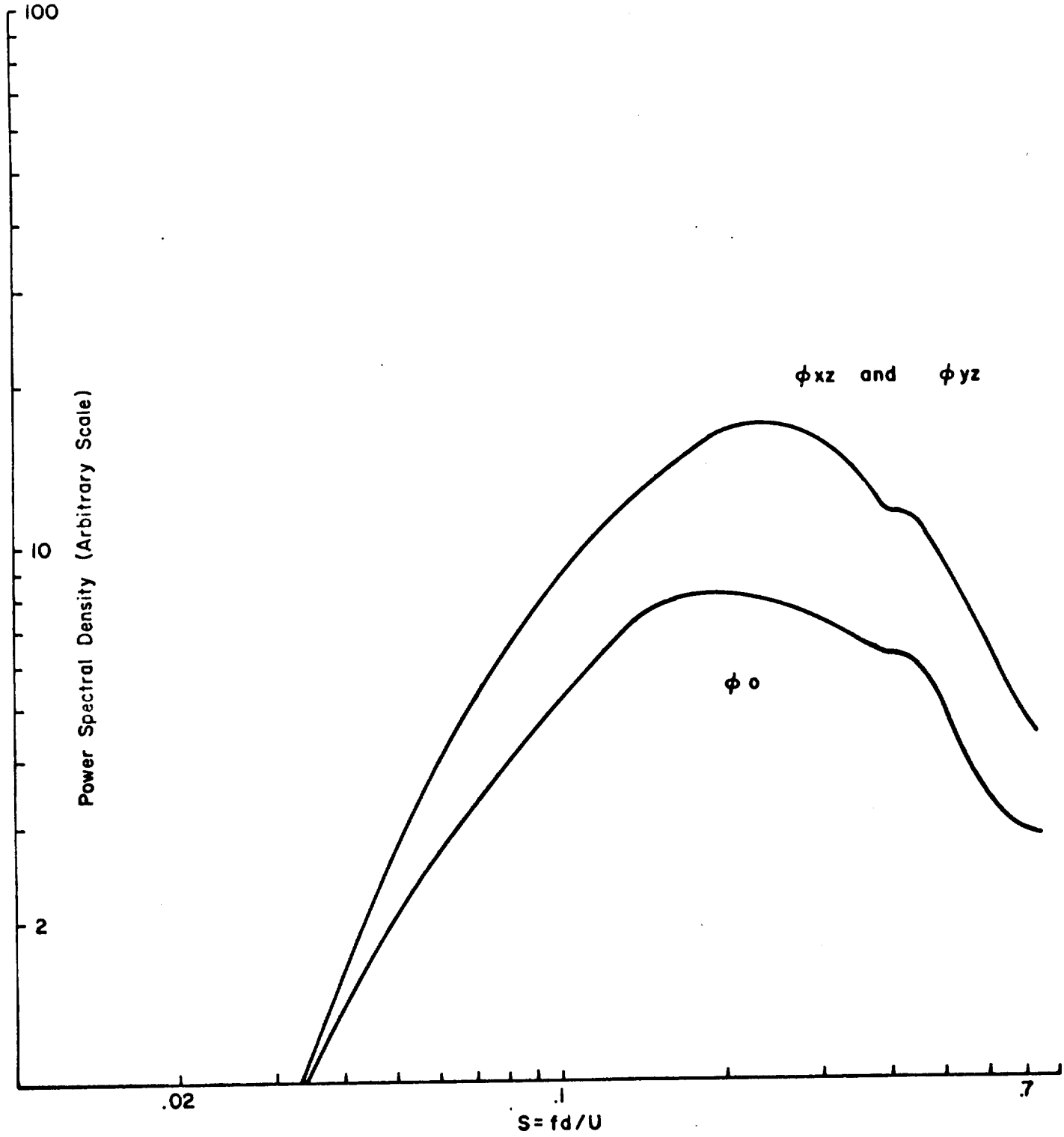

Figure 28 Far Field Spectra Associated With Cylinder Type Turbulence Generator $N = 5.7$ Kc. $r = 30"$, $\beta = 40°$

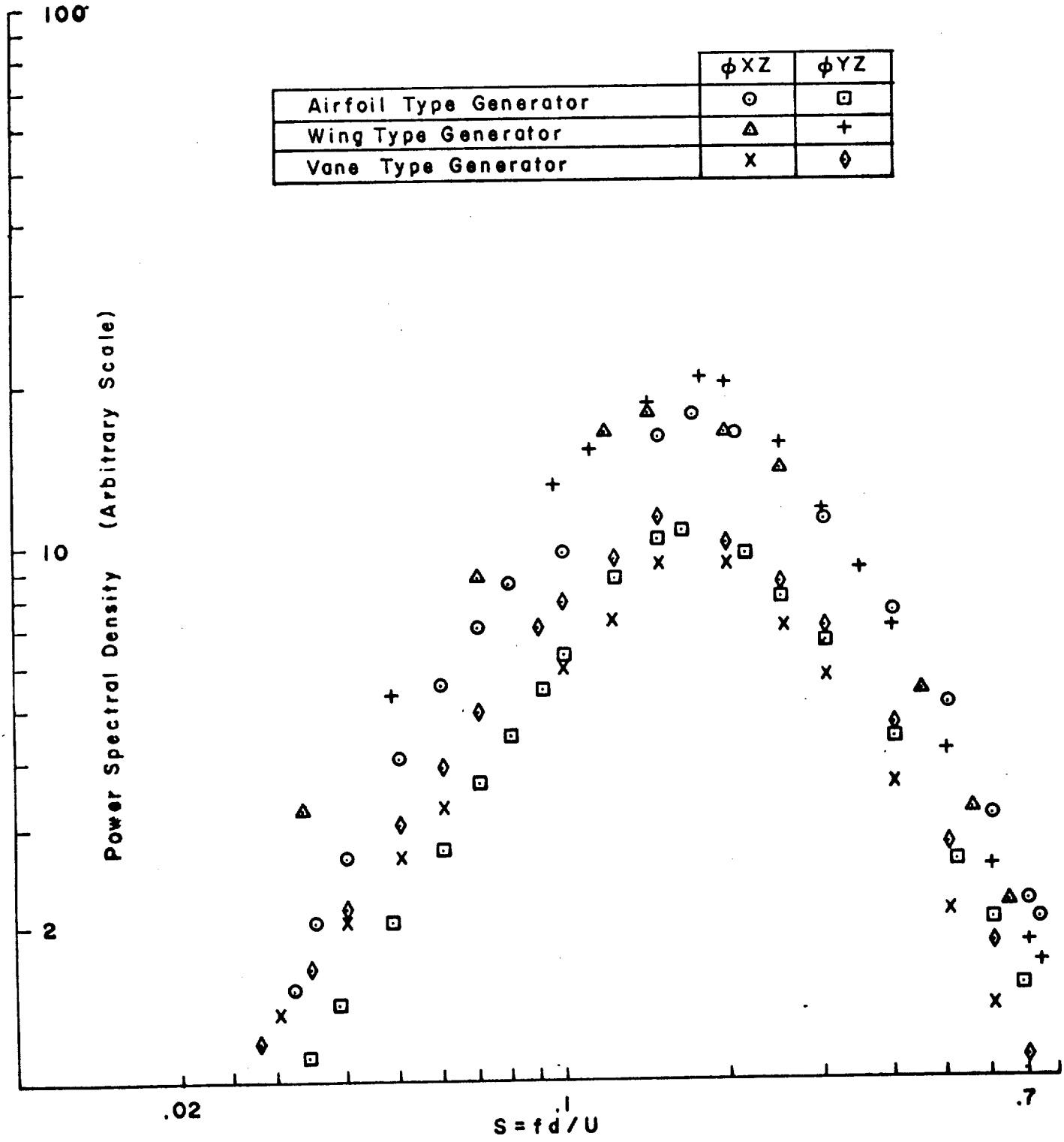

Figure 29 Far Field Spectra Associated With the Airfoil and Vane Type Vortex Generators and the Wing Type Turbulence Generator $r = 36"$, $\beta = 30°$